

AperTO - Archivio Istituzionale Open Access dell'Università di Torino

Novel ureidopropanamide based N-formyl peptide receptor 2 (FPR2) agonists with potential application for central nervous system disorders characterized by neuroinflammation

This is the author's manuscript

Original Citation:

Availability:

This version is available <http://hdl.handle.net/2318/1657279> since 2018-01-12T16:14:23Z

Published version:

DOI:10.1016/j.ejmech.2017.09.023

Terms of use:

Open Access

Anyone can freely access the full text of works made available as "Open Access". Works made available under a Creative Commons license can be used according to the terms and conditions of said license. Use of all other works requires consent of the right holder (author or publisher) if not exempted from copyright protection by the applicable law.

(Article begins on next page)

Novel Ureidopropanamide Based *N*-Formyl Peptide Receptor 2 (FPR2) Agonists with Potential Application for Central Nervous System Disorders Characterized by Neuroinflammation

Madia Letizia Stama,¹ Joanna Ślusarczyk,² Enza Lacivita,^{1*} Liliya N. Kirpotina,³ Igor A. Schepetkin,³ Katarzyna Chamera,² Chiara Riganti,⁴ Roberto Perrone,¹ Mark T. Quinn,³ Agnieszka Basta-Kaim,² Marcello Leopoldo¹

Affiliation

¹Dipartimento di Farmacia - Scienze del Farmaco, Università degli Studi di Bari Aldo Moro, via Orabona, 4, 70125 Bari, Italy

²Department of Experimental Neuroendocrinology, Institute of Pharmacology, Polish Academy of Sciences, 12 Smetna St, 31-343 Krakow, Poland

³Department of Microbiology and Immunology, Montana State University, Bozeman, MT 59717, USA

⁴Dipartimento di Oncologia, Università di Torino, via Santena, 5/bis, 10126 Torino, Italy

*Corresponding Author: Enza Lacivita, Dipartimento di Farmacia – Scienze del Farmaco, Università degli Studi di Bari “Aldo Moro”, via Orabona, 4, 70125, Bari, Italy. E-mail: enza.lacivita@uniba.it; Phone: +39 080 5442750; Fax: +39 080 5442231

Abstract

Formyl peptide receptor-2 (FPR2) is a G protein-coupled receptor belonging to the *N*-formyl receptor family (FPRs) that plays critical roles in peripheral and brain inflammatory responses. FPR2 has been proposed as a therapeutic target for the development of drugs that could facilitate the resolution of pathological inflammatory reactions by enhancing endogenous anti-inflammation systems. Starting from our lead agonist **5**, we have designed new ureidopropanamides derivatives able to activate FPR2 receptors in transfected cells and in human neutrophils. The new FPR2 agonists showed good stability towards oxidative metabolism when incubated with rat microsomes. Moreover, selected compounds were evaluated in an *in vitro* model of neuroinflammation, showing anti-inflammatory properties in rat primary microglial cells after stimulation with lipopolysaccharide (LPS). (*S*)-3-(4-Cyanophenyl)-*N*-[[1-(3-chloro-4-fluorophenyl)cyclopropyl]methyl]-2-[3-(4-fluorophenyl)ureido]propanamide ((*S*)-**17**) emerged as prospective pharmacological tool to study the effects of FPR2 activation in the CNS because it was able to reduce IL-1 β and TNF- α levels in LPS-stimulated microglial cells through specific interaction with FPR2 and showed good permeation rate in hCMEC/D3 cells, an *in vitro* model of blood brain barrier. These results are very promising and can open new therapeutic perspectives in the treatment of those Central Nervous System disorders characterized by neuroinflammation.

Introduction

Neuroinflammation is a complex multicellular process that plays a central role in a variety of neurological diseases, including ischemia, neurodegenerative diseases, psychiatric and immune-mediated disorders.^{1,2} Increasing evidence suggests that microglia, the resident immune cells of the central nervous system (CNS), play a pivotal role in inflammation-associated disorders. Under normal conditions, activation of microglia cells exerts a protective role by regulating the response to pathogens and promoting tissue repair through the release of anti-inflammatory and neurotrophic factors.³ On the other hand, chronic activation of immune responses can lead to the functional switch of microglia from regulatory to neurotoxic leading to the excessive release of pro-inflammatory cytokines, such as IL-1 β , IL-18, and TNF- α , as well as of neurotoxic mediators like nitric oxide (NO), prostaglandin E2, and superoxide anion.⁴ Microglial activation is a phenotypically and functionally dynamic process, which may progress differently depending on aging, stage of disease or on the status of the brain environment.^{5,6}

In general, inflammation requires tight regulation and control: pro-inflammatory mediators operate in a parallel and serial fashion to provoke the classical signs of inflammation, while anti-inflammatory mediators ensure resolution of the inflammatory response. This latter aspect has gained interest in recent years because several classes of peptidic or non-peptidic endogenous factors have been identified as pro-resolving mediators.⁷ Many pro- and anti-inflammatory signals and pro-resolving circuits converge on a group of receptors that integrate contrasting cues to determine the course of inflammation. Among these receptors is the formyl peptide receptor 2 (FPR2),^{8,9} a G-protein coupled receptor that belongs to the formyl peptide receptor (FPR) family, which includes also the subtypes FPR1 and FPR3. FPRs are expressed in several immune cells, including neutrophils, monocytes/macrophages and microglia and are considered to play relevant roles in innate immunity and host defense mechanisms and chemotaxis.⁹ FPR2 is functionally expressed in glial cells and astrocytes.¹⁰⁻¹² FPRs have homologs in fish and rodents.^{13,14} For

example, Fpr2, a homolog of human FPR2, is localized in rat satellite glial cells and neurons of dorsal root ganglions.¹⁵ Recently, expression of Fpr1 and Fpr2 were also reported in rat neuronal stem cells.¹⁶ A prominent and unusual feature of FPR2 is that it can be activated by a variety of structurally diverse agonists. Several endogenous peptides can activate FPR2 and are able to induce very different biological effects. For example, FPR2 can mediate pro-inflammatory effects if activated by *N*-formyl peptides, produced by bacteria and mitochondria to induce defense mechanisms, as well as by the amyloidogenic peptides serum amyloid A, β -amyloid, and prion protein PrP(106-126), which are associated with chronic inflammation and amyloidosis. On the other hand, FPR2 can mediate anti-inflammatory effects if activated by Annexin A1, a glucocorticoid-regulated protein that is involved in the adhesion mechanisms of leukocytes, as well as by lipoxin A4 (LXA₄), which is an anti-inflammatory lipid, the first endogenous FPR2 ligand to be identified.^{9,17} The ability of FPR2 to mediate contrasting effects is mechanistically related to the receptor dimerization that can be induced in a ligand-specific manner.¹⁸

Preclinical evidence generated with pharmacological tools or with knockout and transgenic mice has suggested that LXA₄ contributes to the resolution of inflammation through the activation of FPR2, which in turn modulates chemokine and cytokine synthesis, inhibits neutrophils infiltration, and promotion of phagocytosis.¹⁹⁻²¹ Recently, stimulation of the resolution phase has been proposed as a new therapeutic perspective for the treatment of chronic inflammatory diseases such as chronic obstructive pulmonary disease, cystic fibrosis, rheumatoid arthritis, and also for CNS diseases.^{22,23}

With this respect, recent data demonstrate that LXA₄ inhibits microglial activation and diminishes neuroinflammation after spinal cord hemisection.²⁴ Moreover, in rat hemorrhage, the beneficial role of LXA₄ in suppression of inflammation mediated by FPR2 and p38 MAPK signaling pathways has been demonstrated.²⁵ It is worth emphasizing that the administration of LXA₄ in a transgenic mouse model of Alzheimer's Disease is able to stimulate a pro-resolving activation of microglia by reducing NF- κ B activation and levels of pro-inflammatory cytokines and chemokines and by increasing levels of anti-inflammatory IL-10. This alternative activation of microglia translated into

an improved phagocytic function with increased clearance of β -amyloid plaques, reduced synaptotoxicity, and improvement of cognition.²⁶

A wide range of chemically diverse non-peptidic FPR agonists have been identified so far,²⁷ including benzimidazole derivatives exemplified by compound **1**,²⁸ *N*-phenylurea derivatives (compound **2**),²⁹ quinazolinones derivatives such as the highly specific non-peptide FPR2 agonist Quin-C1 (**3**),³⁰ and pyrazolone derivatives like the mixed FPR1/FPR2 agonist **4** (designated in most of publications as “Compound 43”)³¹ (see Chart 1). Recently, we reported the identification of a group of 3-(1*H*-indol-3-yl)-2-[3-(4-substituted-phenyl)ureido]propanamide derivatives as agonists of human FPR2, exemplified by compound **5** (Table 1, Chart 1).^{32,33} The above agonists were characterized for their ability to induce intracellular Ca^{2+} release. Whereas agonists **3** and **4** exhibited anti-inflammatory properties in peripheral models of inflammation,^{34,35} there are no reports on the effects of FPR2 agonists in *in vitro* or *in vivo* models of neuroinflammation. Based on our previous studies, we aimed to identify new potent FPR2 agonists and to prove if the new ureidopropanamide derivatives display anti-inflammatory and pro-resolving effects in an *in vitro* model of neuroinflammation. Toward this aim, we have modified the structural framework of **5** taking into account that this agonist showed very low stability toward oxidative metabolism and was rapidly degraded after incubation with rat liver microsomes, thus implying that **5** has a pharmacokinetic profile not compatible with *in vivo* studies.³³

Results and Discussion

Study Design. As indicated above, **5** is a potent FPR2 agonist in FPR2-transfected HL-60 cells and in human neutrophils³² but displays very low stability toward oxidative metabolism (Table 1). Thus, in search of metabolically stable FPR2 receptor agonists we selected from our chemical library various 3-(1*H*-indol-3-yl)-2-[3-(4-substituted-phenyl)ureido]propanamide derivatives and tested them for their susceptibility to oxidative metabolism *in vitro* using rat liver microsomes. We

assessed microsomal stability as the percentage of recovery of parent compound after a 30 minutes incubation with liver microsomes preparation, as described previously.³⁶ Among the screened compounds, the enantiomeric pair (*R*)- and (*S*)-**6** had a percentage of recovery (15% and 11%, respectively) higher than that of **5** (4%) (Table 1). Regarding interaction with FPR2, (*R*)-**6** was previously characterized as a weak FPR2 antagonist, whereas (*S*)-**6** was able to induce Ca²⁺ mobilization, albeit with low potency (EC₅₀ = 7.6 μM).³² Therefore, considering the slightly more favorable metabolic stability profile, we selected (*S*)-**6** as starting point for our study with the aim of improving both potency in FPR2 activation and metabolic stability *in vitro*. We systematically evaluated both enantiomers of the target compounds **6-17** (Table 1) because previous studies have shown that the interaction of these chiral ureidopropanamides with FPRs can be highly stereospecific.³² We assessed the ability of the target compounds to induce Ca²⁺ mobilization in HL-60 cells transfected with *h*-FPR1 or *h*-FPR2 receptors and in human neutrophils. Finally, considering that the ability to induce Ca²⁺ mobilization is a feature exhibited by both pro-inflammatory and pro-resolving FPR2 agonists, the compounds showing the best combination of potency and metabolic stability were further characterized in primary rat microglia cultures to assess their anti-inflammatory properties.

Chemistry. Synthesis of the target compounds is depicted in Scheme 1. The key amines **22** and **23** were prepared from the corresponding nitriles **18** and **19**^{37,38} after hydrogenation over Nickel-Raney. The amine **24** was prepared by reduction of nitrile **20**³⁹ with the borane-dimethyl sulfide complex in order to avoid reductive dehalogenation. The amines **21-24** were then condensed with the appropriate (*R*)-Boc- or (*S*)-Boc-amino acids **25-27** after activation with *N*-*N'*-carbonyldiimidazole to give the Boc-protected derivatives (*R*)- and (*S*)- **28-33**. Subsequently, these latter compounds were deprotected with trifluoroacetic acid to give amines (*R*)- and (*S*)- **34-39**. The target compounds were obtained by condensing amines (*R*)- and (*S*)- **34-39** with the appropriate phenylisocyanate, except for compounds (*R*)-**8**, (*S*)-**14**, (*S*)-**15**, and (*R*)-**17**, that were prepared by

condensing the amines (*R*)-**34**, (*S*)-**38**, (*R*)-**39** with the the appropriate aniline and *N-N'*-carbonyldiimidazole.

Intrinsic Activity and Metabolic Stability of the Target Compounds. The first structural modification on (*R*)- and (*S*)-**6** was removal of the nitro substituent from the phenylureidic group or its replacement with –OCH₃ or –F substituents. This structural modification was inspired by previous structure-activity relationship studies on ureidopropanamide derivatives, where the introduction of a methoxy group³² or an halogen⁴⁰ in the same position led to an improvement in agonist potency. Indeed, (*S*)-**7** and (*S*)-**8** showed EC₅₀ values lower than that of (*S*)-**6**. The effect was more pronounced for the methoxy derivative (*S*)-**7** (Table 1). In contrast, removal of the nitro substituent of (*S*)-**6** had little impact on its potency ((*S*)-**9**). Interestingly, replacement of the nitro group with a methoxy group in (*R*)-**6** shifted the intrinsic activity from antagonism to agonism ((*R*)-**7**).³² This effect was not observed for derivatives (*R*)-**8** and (*R*)-**9**, which were not able to induce Ca²⁺ mobilization. It can be noted that the replacement of the nitro group with other substituents led to a decrease of selectivity towards FPR1, being (*S*)-**7**, (*S*)-**8**, and (*S*)-**9** able to activate FPR1 receptors as well. In particular, (*S*)-**9** showed a slight preference for FPR1 over FPR2. Finally, similarly to (*S*)-**6**, (*S*)-**8** and (*S*)-**9** behaved as partial agonists, whereas (*S*)-**7** was characterized as a full agonist at both FPR1 and FPR2.

Considering metabolic stability, it can be noted that this structural modification had a negative influence, as the compounds (*R*)- and (*S*)-**7-9**, were less stable than (*R*)- and (*S*)-**6** (Table 1). By comparing compounds **6** and **8**, it can be speculated that the electronic properties of the substituent on the phenyl ureidic moiety can have limited effects on metabolic stability of this group of compounds.

We next evaluated the impact on both potency and metabolic stability of replacement of the tryptophan core in (*R*)- and (*S*)-**6** with that of unnatural amino acids. For this purpose, we selected the commercially available 4-cyanophenylalanine and 3-pyridylalanine. In general, this structural

modification was beneficial. In fact, the introduction of 4-cyanophenylalanine led to a 10-fold increase of agonist potency, as shown by (*S*)-**10** compared to (*S*)-**6**, whereas (*S*)-**11**, which bears the 3-pyridylalanine core, was only slightly more potent than (*S*)-**6** (Table 1). When comparing the (*R*)-enantiomers with (*R*)-**6**, a shift from antagonism to agonism was observed, as (*R*)-**10** and (*R*)-**11** were able to induce Ca²⁺ mobilization although with lower potency than the (*S*)-enantiomers. It can be also noted that (*R*)- and (*S*)-**10** behaved as full agonists, whereas (*R*)- and (*S*)-**11** were characterized as partial agonists. Finally, this structural modification led to substantial increase of FPR1 agonist activity; in particular, (*S*)-**11** showed EC₅₀ value for FPR1 in the low micromolar range. As for metabolic stability, both enantiomeric pairs showed a percentage of recovery higher than 40%, with (*S*)-**10** being the most stable compound of the set (56% recovery) (Table 1). These data suggest that replacement of the tryptophan with an unnatural amino acid led to unfavorable interactions of the molecule with the metabolic enzymes.

On the basis of these data, we selected the 4-cyanophenylalanine as the amino acid core for further modifications to obtain new ureidopropanamide FPR2 agonists. First, we replaced the nitro substituent of (*R*)- and (*S*)-**10** with –OCH₃ or –F with the aim of increasing agonist potency. Additionally, we decorated the phenyl ring on the “right hand” of (*R*)- and (*S*)-**10** with substituents that could prevent interaction of the molecule with metabolic enzymes in an effort to further increase metabolic stability (compounds **12-17**). These modifications did not lead to improved FPR2 agonist potency. In particular, the presence of a substituent in the 4-position of the phenyl linked to the cyclopropyl ring negatively influenced the ability of these compounds to activate FPR2 receptor (Table 1). This effect was more evident for compounds (*R*)- and (*S*)-**12** and (*R*)- and (*S*)-**13**, which feature the bulky trifluoromethoxy group. Instead, (*R*)- and (*S*)-**16** and (*R*)- and (*S*)-**17**, bearing the small F– substituent in 4-position, showed EC₅₀ values comparable to those of (*R*)- and (*S*)-**10** (Table 1). Moreover, the decoration of the phenyl ring linked to the cyclopropyl moiety had different impact on FPR1 interaction, being (*R*)- and (*S*)-**16** potent FPR1 full agonists.

Introduction of bulky substituents on the phenyl linked to the cyclopropyl ring had a beneficial effect on metabolic stability. In fact, derivatives (*R*)- and (*S*)-**13** showed very high percentage recovery (> 80%) (Table 1). However, the methoxy-substituted derivatives showed lower stability than that of the fluoro-substituted counterparts. On the other hand, the presence of the unnatural amino acid core did not always translate into an improvement of metabolic stability. Derivatives (*R*)- and (*S*)-**14**, and (*R*)- and (*S*)-**16** showed metabolic stabilities comparable to those of ureidopropanamides with the tryptophan core (Table 1).

Collectively, these data clearly indicate that the “right hand” of these ureidopropanamides plays an important role in the interaction with FPR2 receptor because structural modifications in this part of the molecule greatly influence agonist potency. On the other hand, the steric hindrance of this part of the molecule seems to be an important requisite for metabolically stable compounds. Therefore, it is important to find the right balance in the dimension of the cyclopropyl phenyl moiety in order to combine high potency with good metabolic stability.

We next evaluated the ability of the new compounds to activate FPR2 in human neutrophils. The data show that neutrophils responded to all agonists that activated FPR-expressing HL-60 cells. The only exceptions were (*R*)-**8** and (*R*)-**9**, which were able to induce Ca²⁺ mobilization in neutrophils but not in FPR-expressing HL-60 cells. Among the studied compounds, (*R*)-**11** and (*S*)-**17** showed EC₅₀ values in the submicromolar range.

Half-life and Intrinsic Clearance of Selected Compounds. According to our paradigm for assessing metabolic stability of the new compounds, derivatives (*R*)- and (*S*)-**10**, (*R*)- and (*S*)-**11**, (*R*)-**15**, (*R*)- and (*S*)-**17**, which all showed recovery higher than 20%, were further characterized by evaluating half-life ($t_{1/2}$) and intrinsic clearance (CL_{int}) (Table 2). All selected compounds showed CL_{int} much lower than that of **5**, confirming that the new derivatives were more stable than **5** with respect to microsomal oxidative metabolism. Moreover, all compounds displayed $t_{1/2}$ values exceeding 15 min, which is reported as the lower limit for predicted low clearance compounds.⁴¹

Among the new compounds, (*S*)-**10**, (*R*)-**11**, and (*S*)-**17** showed a good balance between potency and metabolic stability and were, thus, selected for further studies in order to assess their pharmacological properties in an *in vitro* model of neuroinflammation.

Effect of Selected Compounds on Cell Viability and Metabolic Activity in Rat Primary

Microglial Cells. Initially, we evaluated the effect of (*S*)-**10**, (*R*)-**11**, and (*S*)-**17** on cell viability and metabolic activity in rat primary microglia cell cultures under basal conditions and after stimulation with lipopolisaccharide (LPS). It is well known that LPS is a primary component of endotoxin from Gram-negative bacteria cell walls,^{42,43} which binds mostly to Toll-like receptor 4 and induces intracellular signaling resulting in the activation of mitogen activated protein kinases (MAPKs) and NF- κ B.⁴⁴ These proteins have been described as the key regulators of pro-inflammatory factors production such as cytokines and NO, which may have cytotoxic effects and may damage cells.⁴⁵

We evaluated the effect of (*S*)-**10**, (*R*)-**11**, and (*S*)-**17** on cell viability by using the lactate dehydrogenase (LDH) and MTT tests, two biochemical assays that evaluate different aspects of cell death/viability processes. The LDH assay is a well-accepted paradigm to quantitatively assess cell death after damage of the plasma membrane, which results in increased LDH efflux from injured cells, and it is known that LPS induces impairments in cell membrane integrity. On the other hand, MTT test quantifies mitochondrial activity by measuring the formation of a dark blue formazan product formed by reduction of the tetrazolium ring of MTT in living cells. Thus, these tests provide an accurate and complete assessment of the impact of the selected compounds on the vital status of microglial cells in culture.

We first tested the effect of (*S*)-**10**, (*R*)-**11**, and (*S*)-**17** at different doses under basal conditions. None of the compounds induced significant effects on LDH release or metabolic activity in the dose range of 0.5-10 μ M. On the other hand, exposure of the microglial cells to a 50 μ M dose of all compounds resulted in a significant increase in death processes. (*S*)-**10** and (*S*)-**17** also decreased the conversion of MTT dye at a 50 μ M dose (Figure 1).

Next, we evaluated the effect of the selected compounds after stimulation of the microglial cells with LPS, which induces cell death processes by increasing LDH release as well as diminishing metabolic activity. Interestingly, pre-treatment with (*S*)-**10**, (*R*)-**11**, and (*S*)-**17** effectively blocked LPS-induced cell death processes at the doses of 1 μ M and 5 μ M (Figure 1). On the other hand, no effect was observed on metabolic activity in LPS-stimulated microglial cell cultures (Figure 1). These data indicate that (*S*)-**10**, (*R*)-**11**, and (*S*)-**17** did not induce either pro-inflammatory responses or cytotoxicity in microglial cells. Moreover, our FPR2 agonists showed protective properties against LPS treatment in the LDH assays.

Effect of Selected Compounds on Pro-Inflammatory Mediators Production in Rat Primary Microglial Cells. To further characterize the anti-inflammatory properties of our FPR2 agonists, we assessed their effect on the production of the pro-inflammatory mediators NO, IL-1 β and TNF- α in rat primary microglial cell cultures. Under normal conditions, NO is involved in many physiological processes in the brain, such as regulation of proliferation, survival, differentiation of the neurons, synaptic activity, and neural plasticity.⁴⁶ However, excessive NO synthesis leads to the formation of reactive nitrogen species and neuronal cell death. Moreover, there is an intimate relation between microglial activation, NO production, and neuroinflammation in the brain.⁴⁷ Also, inflammatory cytokines, such as IL-1 β and TNF- α , have physiological functions in the brain which include effects on neurite outgrowth, neurogenesis, neuronal survival, and synaptic pruning during brain development, synaptic transmission and synaptic plasticity.⁴⁸ However, overproduction and exaggerated release of cytokines is associated with neuronal dysfunction.

We evaluated effects of the selected FPR2 agonists on the production of NO, IL-1 β , and TNF- α in rat primary microglial cultures under basal conditions and after stimulation with LPS. Furthermore, to check if the observed effect is mediated through the interaction with FPR2, the microglia cells were also pre-treated with the selective FPR2 antagonist WRW4.

(*S*)-**10**, (*R*)-**11**, and (*S*)-**17** did not induce any change in NO level under basal conditions. The same effect was observed when the cells were treated with WRW4 alone or in combination with the selected agonists (Figure 2). Stimulation of the microglial cells with LPS increased the level of NO, which was significantly attenuated by (*S*)-**10** (5 μ M and 10 μ M), whereas no effect was observed for (*R*)-**11** and (*S*)-**17**. Moreover, pre-treatment of the microglial cells with WRW4 was not able to reverse the anti-inflammatory effect on NO secretion evoked by (*S*)-**10**, suggesting that this effect was mediated by the interaction with molecular targets different from FPR2 (Figure 2).

(*S*)-**10**, (*R*)-**11**, and (*S*)-**17** (0.5 μ M-10 μ M) did not induce any change in the intracellular levels of IL-1 β and TNF- α production under basal conditions. As observed for NO production, the antagonist WRW4, alone or in combination with the selected agonists did not affect IL-1 β and TNF- α production (Figures 3 and 4). Consistent with our previous studies, the stimulation with LPS induced a significant up-regulation of both IL-1 β and TNF- α production in the microglial cells.³ Interestingly, (*S*)-**10**, (*R*)-**11**, and (*S*)-**17** showed anti-inflammatory effects, being able to effectively decrease LPS-evoked cytokine production (Figure 3 and 4). Pre-treatment with the antagonist WRW4 was able to block the effect of (*S*)-**17** on both IL-1 β and TNF- α secretion, and of (*R*)-**11** only on IL-1 β production. In the case of (*S*)-**10**, WRW4 did not abolish the observed effect on both pro-inflammatory cytokine release, suggesting that the anti-inflammatory effects of (*S*)-**10** were mediated by other molecular targets (Figure 3 and 4). Considering that the inhibition of IL-1 β and TNF- α production by (*S*)-**17** did not show a clear dose response in the range from 0.5 to 10 μ M, we tested the effect of (*S*)-**17** at lower doses. The data indicated that at 0.05 μ M (*S*)-**17** was not able to induce a significant effect on IL-1 β and TNF- α production, whereas 0.1 μ M (*S*)-**17** showed a clear inhibition effect that was blocked by pre-treatment with the antagonist WRW4, albeit less strong than the effect observed at 0.5 μ M dose (Figure 5).

Collectively, the data indicated that the selected FPR2 agonists did not induce pro-inflammatory responses in resting microglial cells but exerted clear anti-inflammatory effects in the LPS-

stimulated cells. In the case of (*S*)-**17** the anti-inflammatory effect was mediated by FPR2, whereas (*S*)-**10** and (*R*)-**11** seem to exert these effects through other molecular targets.

Evaluation of Permeability in hCMEC/D3 Cells.

A critical characterization for prospective CNS-acting drugs is the ability to cross the blood brain barrier (BBB), which acts as a highly lipophilic boundary. Compounds permeate BBB mainly by passive diffusion mechanism, and several efflux systems prevent the entrance of xenobiotics into CNS. To endorse the potential of compounds (*S*)-**10**, (*R*)-**11**, and (*S*)-**17** as promising leads for the development of neuroprotective agents, *in vitro* transport studies were undertaken. To this end, we selected hCMEC/D3 cells, an immortalized human brain microvascular endothelial cell line, as an *in vitro* model of BBB. hCMEC/D3 cells stably maintain most of the unique structural and biochemical properties of brain endothelium *in vivo*, including tight junctions formation and the expression of multiple efflux transporters of the ABC cassette superfamily.⁴⁹

The permeation rate of compounds (*S*)-**10**, (*R*)-**11**, and (*S*)-**17** across the cell monolayer in both directions, i.e., apical-to-basolateral (AB) and basolateral-to-apical (BA), was assessed (Table 3). Moreover, we evaluated the efflux ratio (ER) between BA and AB fluxes because ER greater than 3 can be taken as a figure of undesirable interaction with the efflux transporters⁵⁰ (Table 3).

Compound (*S*)-**17** showed good permeation rates in both directions and ER value below 3, thus envisaging good brain distribution and low interactions with the efflux transporters. On the other hand, (*S*)-**10** and (*R*)-**11** showed lower permeation rates, especially in AB direction, which is more strongly influenced by the interaction with the efflux transporters, suggesting that (*S*)-**10** and (*R*)-**11** might have low brain distribution.

Conclusion

In summary, we have manipulated the structure of **5**, a potent ureidopropanamide FPRs agonist previously studied in our laboratories, with the aim of identifying new potent FPR2 agonists

endowed with enhanced metabolic stability. Several of these new studied derivatives exhibited agonist potency comparable to that of **5** and significantly higher $t_{1/2}$ and CL_{int} , indicating that the aim of improving stability towards oxidative metabolism was achieved. Analysis of (*S*)-**10**, (*R*)-**11**, and (*S*)-**17** in an *in vitro* model of neuroinflammation showed that they did not induce inflammatory responses in resting rat primary microglial cell cultures but they were able to significantly reduce the production of pro-inflammatory mediators when microglial cells were stimulated with LPS. In particular, compound (*S*)-**17** was able to reduce IL-1 β and TNF- α levels in LPS-stimulated microglial cells and this effect was mediated by FPR2 interaction because its effects were blocked by pre-treatment of the cells with the FPR2 antagonist WRW4. Moreover, bidirectional transport studies on hCMEC/D3 cells denoted good permeation rates of compound (*S*)-**17** without suffering from likely efflux transporters interactions, thus suggesting good brain permeation and CNS distribution.

To the best of our knowledge, this is the first report on FPR2 agonists being studied in a model of neuroinflammation in order to evaluate their ability to induce anti-inflammatory responses in primary microglial cells. Among the studied agonists, (*S*)-**17** emerges as a prospective pharmacological tool to study the effects of FPR2 activation in the CNS because it elicits FPR2-mediated anti-inflammatory effects in rat microglia and also displays suitable pharmacokinetic characteristics. We believe that these data are promising considering that very recent studies have indicated that stimulation of brain FPR2 with endogenous ligands such as LXA1 or Annexin A1 (Ries)⁵¹ is able to inhibit microglial activation and diminish neuroinflammation in several pathological conditions, including Alzheimer's Disease and neuropathic pain. This can open new therapeutic perspectives in the treatment of those CNS disorders characterized by neuroinflammation.

Experimental Section

Chemistry. Chemicals were purchased from Sigma-Aldrich, Alfa Aesar, TCI Chemicals. Unless otherwise stated, all chemicals were used without further purification. Thin layer chromatography (TLC) was performed using plates from Merck (silica gel 60 F254). Column chromatography was performed with 1:30 Merck silica gel 60 Å (63-200 μm) as the stationary phase. Flash chromatographic separations were performed on a Biotage SP1 purification system using flash cartridges pre-packed with KP-Sil 32–63 μm, 60 Å silica. ¹H NMR spectra were recorded on a Varian Mercury-VX spectrometer (300 MHz) or on a 500-nmrs500 Agilent spectrometer (500 MHz). All chemical shift values are reported in ppm (δ). For enantiomeric pairs, NMR spectra for both enantiomers were recorded but the NMR spectrum of only the (*R*)-enantiomer is reported in the experimental section. Recording of mass spectra was done on an HP6890-5973 MSD gas chromatograph/mass spectrometer; only significant *m/z* peaks, with their percentage of relative intensity in parentheses, are reported. HRMS-ESI analyses were performed on a Bruker Daltonics MicroTOF-Q II mass spectrometer, mass range 50-800 *m/z*, electrospray ion source in positive or negative ion mode. All spectra were in accordance with the assigned structures. The purity of the target compounds listed in Table 1 was assessed by RP-HPLC and combustion analysis. All compounds showed ≥ 98% purity. RP-HPLC analysis was performed on an Agilent 1260 Infinity Binary LC System equipped with a diode array detector using a Phenomenex Gemini C-18 column (250 x 4.6 mm, 5 μm particle size). All target compounds (Table 1) were eluted with CH₃OH/H₂O/Et₃N, 8:2:0.01 at a flow rate of 1 mL/min. Elemental analyses (C,H,N) of the target compounds were performed on a Eurovector Euro EA 3000 analyzer. Analyses indicated by the symbols of the elements were within ± 0.4 % of the theoretical values. Enantiomeric purity of the target compounds (*R*)- and (*S*)-**6-17** was assessed by chiral HPLC analysis on a Perkin-Elmer series 200 LC instrument using a Daicel ChiralCel OD column (250 mm × 4.6 mm, 5 μm particle size) and equipped with a Perkin-Elmer 785A UV/VIS detector setting λ= 230 nm. The compounds were eluted with *n*-hexane/EtOH, 4:1, v/v at a flow rate of 0.8 mL/min. All compounds showed enantiomeric excesses ≥ 98%.

The following compounds were prepared according to literature methods: 1-[(4-trifluoromethoxy)phenyl]cyclopropanecarbonitrile (**18**);³⁷ 1-(3-chloro-4-fluorophenyl)-cyclopropanecarbonitrile (**19**);³⁸ 1-(3-fluoro-4-methylphenyl)-cyclopropanecarbonitrile (**20**);³⁹ 1-(phenylcyclopropyl)methylamine (**21**).⁵²

General Procedure for the Synthesis of the Amines 22 and 23.

Raney nickel was activated with 10 M KOH, then washed with H₂O, then with EtOH to remove H₂O. The catalyst was then taken up in 2 N ethanolic ammonia and the appropriate nitrile (0.87 mmol) was added to the mixture which was then hydrogenated under 5 bar pressure of hydrogen at 50 °C for 15 h. The reaction mixture was then filtered through Celite and concentrated *in vacuo* to give the desired amine as an oil.

[1-(4-Trifluoromethoxyphenyl)cyclopropyl]methanamine (22).

90% Yield. ¹H NMR (CDCl₃): δ 0.74-0.83 (m, 4H), 1.35 (br s, 2H), 2.76 (s, 2H), 7.13 (d, 2H, *J* = 8.3 Hz), 7.27 (d, 2H, *J* = 8.1 Hz). GC/MS: *m/z* 231 (M⁺, 7), 203 (100), 134 (67), 115 (35).

[1-(3-Fluoro-4-methylphenyl)cyclopropyl]methanamine (23).

77% Yield. ¹H NMR (CDCl₃): δ 0.72–0.81 (m, 4H), 1.35 (br s, 2H), 2.23 (s, 3H), 2.74 (s, 2H), 6.74–6.82 (m, 2H), 7.07 (t, 1H, *J*_{H-H} = 7.6 Hz, *J*_{H-F} = 8.2 Hz), GC/MS: *m/z* 179 (M⁺, 25), 151 (100), 147 (36), 133 (49), 109 (37).

[1-(3-Chloro-4-fluorophenyl)cyclopropyl]methanamine (24).

Borane-methyl sulfide complex as 10.0 M BH₃ in excess methyl sulfide (4.6 mmol, 0.46 mL) was dropped into an ice-cooled solution of 1-(3-chloro-4-fluorophenyl)cyclopropylcarbonitrile (0.30 g, 1.5 mmol) in anhydrous THF (10 mL), under stirring. After being refluxed for 3-4 h, the reaction mixture was cooled at -10 °C and MeOH was added dropwise very carefully until gas evolution

ceased. The mixture was treated with 3 N HCl (20 mL) and was refluxed for 1 h. After cooling, the mixture was alkalized with 3 N NaOH and extracted with CH₂Cl₂ (5 × 20 mL). The collected organic layers were dried over Na₂SO₄ and the solvent was evaporated under pressure to give the pure amine as a colorless oil (0.25 g; 81% yield). ¹H NMR (CDCl₃): δ 0.73–0.82 (m, 4H), 1.37 (br s, 2H), 2.76 (s, 2H), 7.07 (t, 1H, *J*_{H-H} = 8.2 Hz, *J*_{H-F} = 8.8 Hz), 7.17–7.22 (m, 1H), 7.36 (dd, 1H, *J* = 7.0, 2.3 Hz). GC/MS: *m/z* 201 (M⁺+2, 1), 199 (M⁺, 4), 171 (100), 147 (27), 133 (60), 109 (29).

General Procedure for the Synthesis of Boc-protected Derivatives (*R*)- and (*S*)-28–33.

N,N'-Carbonyldiimidazole (1.1 mmol) was added to a solution of (*R*)- or (*S*)-Boc-protected amino acid (1.0 mmol), in anhydrous THF (10 mL) under N₂. The reaction mixture was stirred at room temperature overnight, then a solution of the appropriate amine (1.0 mmol) in anhydrous THF was added. The reaction mixture was stirred at room temperature for 6 h. Then, the solvent was removed *in vacuo* and the residue was partitioned between EtOAc (20 mL) and H₂O (2 × 20 mL). The aqueous layer was separated and extracted twice with EtOAc (20 mL). The collected organic layers were dried (Na₂SO₄) and evaporated *in vacuo*. The crude residue was purified through flash chromatography (gradient elution from 30% to 70% ethyl acetate in *n*-hexane) to give pure target compound as a white solid.

(*R*)-1-(1*H*-Indol-3-ylmethyl)-2-[[1-(phenylcyclopropyl)methyl]amino]-2-oxoethyl]carbamic acid, 1,1-Dimethylethyl Ester ((*R*)-28).

58% Yield. ¹H NMR (CDCl₃): δ 0.62–0.76 (m, 4H), 1.40 (s, 9H), 3.08 (dd, 2H, *J* = 14.4, 8.2 Hz), 3.31 (dd, 2H, *J* = 13.8, 5.2 Hz), 4.35–4.37 (m, 1H), 5.13 (br s, 1H), 5.63 (br s, 1H), 6.90–6.92 (m, 3H), 7.11–7.16 (m, 3H), 7.22 (dt, 2H, *J* = 6.9, 1.1 Hz), 7.36 (d, 1H, *J* = 8 Hz), 7.65 (d, 1H, *J* = 8 Hz), 8.02 (br s, 1H). ESI/MS *m/z* 432 (M-H)⁻, ESI-MS/MS *m/z* 358 (100), 229 (68).

(*S*)-1-(1*H*-Indol-3-ylmethyl)-2-[[1-(phenylcyclopropyl)methyl]amino]-2-oxoethyl]carbamic acid, 1,1-Dimethylethyl Ester ((*S*)-28).

72% Yield. ESI/MS m/z 432 (M-H)⁻, ESI-MS/MS m/z 358 (100), 229 (63).

(R)-1-(4-Cyanophenylmethyl)-2-[[1-(1-phenylcyclopropyl)methyl]amino]-2-oxoethyl]carbamic acid, 1,1-Dimethylethyl Ester ((R)-29).

75% Yield. ¹H NMR (CDCl₃): δ 0.76–0.89 (m, 4H), 1.38 (s, 9H), 2.96 (dd, 1H, J = 13.5, 6.4 Hz), 3.07 (dd, 1H, J = 13.5, 7.6 Hz), 3.32 (dd, 1H, J = 14.1, 5.9 Hz), 3.4 (dd, 1H, J = 14.1, 5.9 Hz), 4.23–4.27 (m, 1H), 4.98 (br d, 1H), 5.8 (br t, 1H), 7.12–7.15 (m, 2H), 7.20–7.31 (m, 5H), 7.51 (d, 2H, J = 8.8 Hz). ESI⁺/MS m/z 442 (M+Na)⁺, ESI⁺/MS/MS m/z 342 (100).

(S)-1-(4-Cyanophenylmethyl)-2-[[1-(1-phenylcyclopropyl)methyl]amino]-2-oxoethyl]carbamic acid, 1,1-Dimethylethyl Ester ((S)-29).

64% yield. ESI⁺/MS m/z 442 (M+Na)⁺, ESI⁺/MS/MS m/z 342 (100).

(R)-2-[[1-(1-Phenylcyclopropyl)methyl]amino]-2-oxoethyl]-1-(3-pyridinylmethyl)carbamic acid, 1,1-Dimethylethyl Ester ((R)-30).

58% Yield. ¹H NMR (CDCl₃): δ 0.80–0.85 (m, 4H), 1.37 (s, 9H), 2.93 (dd, 1H, J = 13.5, 7.0 Hz), 3.04 (dd, 1H, J = 14.1, 7.0 Hz), 3.38 (d, 2H, J = 5.3 Hz), 4.20–4.25 (m, 1H), 4.97 (br d, 1H), 5.91 (br t, 1H), 7.13–7.20 (m, 5H), 7.23–7.26 (m, 1H), 7.46 (d, 1H, J = 7.6 Hz), 8.39 (d, 1H, J = 1.8 Hz), 8.47 (dd, 1H, J = 4.7, 1.2 Hz). ESI⁺/MS m/z 418 (M+Na)⁺, ESI⁺/MS/MS m/z 318 (100).

(S)- 2-[[1-(1-Phenylcyclopropyl)methyl]amino]-2-oxoethyl]-1-(3-pyridinylmethyl)carbamic acid, 1,1-Dimethylethyl Ester ((S)-30).

45% Yield. ESI⁺/MS m/z 418 (M+Na)⁺, ESI⁺/MS/MS m/z 318 (100).

(R)-1-(4-Cyanophenylmethyl)-2-[[[1-(4-trifluoromethoxyphenyl)cyclopropyl]methyl]amino]-2-oxoethyl]carbamic acid, 1,1-Dimethylethyl Ester ((R)-31).

84% Yield. ¹H NMR (CDCl₃): δ 0.79–0.89 (m, 4H), 1.38 (s, 9H), 2.99 (dd, 1H, J = 13.5, 6.5 Hz), 3.13 (dd, 1H, J = 13.5, 7.0 Hz), 3.35 (dd, 1H, J = 13.5, 5.5 Hz), 3.42 (dd, 1H, J = 13.5, 5.5 Hz); 4.26–

4.27 (m, 1H), 4.87 (br s, 1H), 5.92 (br t, 1H), 7.13 (d, 2H, $J = 8.5$ Hz), 7.19–7.21 (m, 2H), 7.26–7.28 (m, 2H), 7.57 (d, 2H, $J = 8.5$ Hz). ESI⁺/MS: m/z 526 (M+Na)⁺, ESI⁺-MS/MS: m/z 426 (100).

(S)-1-(4-Cyanophenylmethyl)-2-[[[(1-(4-trifluoromethoxyphenyl)cyclopropyl)methyl]amino]-2-oxoethyl]carbamic acid, 1,1-Dimethylethyl Ester ((S)-31).

87% Yield. ESI⁺/MS: m/z 526 (M+Na)⁺. ESI⁺-MS/MS: m/z 426 (100).

(R)-1-(4-Cyanophenylmethyl)-2-[[[(1-(3-fluoro-4-methylphenyl)cyclopropyl)methyl]amino]-2-oxoethyl]carbamic acid, 1,1-Dimethylethyl Ester ((R)-32).

81% Yield. ¹H NMR (CDCl₃): δ 0.75–0.84 (m, 4H), 1.38 (s, 9H), 2.23 (s, 3H), 2.98 (dd, 1H, $J = 13.5, 6.6$ Hz); 3.10 (dd, 1H, $J = 13.5, 6.5$ Hz); 3.34 (d, 2H, $J = 5.4$ Hz); 4.20–4.25 (m, 1H), 4.94 (br d, 1H), 5.84 (br t, 1H), 6.74–6.82 (m, 2H), 7.07 (t, 1H, $J = 8.0$ Hz), 7.25 (d, 2H, $J = 8.4$ Hz), 7.55 (d, 2H, $J = 8.1$ Hz). ESI⁺/MS: m/z 474 (M+Na)⁺; ESI⁺-MS/MS: m/z 374 (100).

(S)-1-(4-Cyanophenylmethyl)-2-[[[(1-(3-fluoro-4-methylphenyl)cyclopropyl)methyl]amino]-2-oxoethyl]carbamic acid, 1,1-dimethylethyl ester ((S)-32).

71% Yield. ESI⁺/MS: m/z 474 (M+Na)⁺, ESI⁺-MS/MS: m/z 374 (100).

(R)-2-[[[(1-(3-Chloro-4-fluorophenyl)cyclopropyl)methyl]amino]-2-oxoethyl]-1-(4-cyanophenylmethyl)-carbamic acid, 1,1-Dimethylethyl Ester ((R)-33).

77% Yield. ¹H NMR (CDCl₃): δ 0.78–0.89 (m, 4H), 1.39 (s, 9H), 2.98 (dd, 1H, $J = 13.5, 7.0$ Hz), 3.13 (dd, 1H, $J = 13.5, 7.0$ Hz), 3.32 (dd, 1H, $J = 14.0, 5.5$ Hz), 3.38 (dd, 1H, $J = 14.0, 5.5$ Hz), 4.24–4.28 (m, 1H), 4.94 (br s, 1H), 6.04 (br t, 1H), 7.02–7.06 (m, 2H), 7.20 (d, 1H, $J = 7.0$ Hz), 7.28 (d, 2H, $J = 8.5$ Hz), 7.58 (d, 2H, $J = 8.0$ Hz). ESI⁺/MS: m/z 494 (M+Na)⁺, ESI⁺-MS/MS: m/z 394 (100).

(S)- 2-[[[(1-(3-Chloro-4-fluorophenyl)cyclopropyl)methyl]amino]-2-oxoethyl]-1-(4-cyanophenylmethyl)-carbamic acid, 1,1-Dimethylethyl Ester ((S)-33).

84% Yield. ESI⁺/MS: m/z 494 (M+Na)⁺, ESI⁺-MS/MS: m/z 394 (100).

General Procedure for the Synthesis of Amines (R)- and (S)-34–39.

Trifluoroacetic acid (5 mL) was added to a solution of Boc-protected derivatives (R)- and (S)-29-33 (0.46 mmol) in CH₂Cl₂ (20 mL). The reaction mixture was stirred at room temperature for 5 h and basified with aqueous 1 M NaOH. The separated aqueous phase was extracted with CH₂Cl₂ (2 × 20 mL). The combined organic layers were dried (Na₂SO₄) and concentrated *in vacuo* to give the desired compounds as pale yellow semisolids that were used without further purification.

(R)-2-Amino-3-(1H-indol-3-yl)-N-[(1-phenylcyclopropyl)methyl]propanamide ((R)-34).

97% Yield. ¹H NMR (CDCl₃): δ 0.81–0.88 (m, 4H), 1.45 (br s, 2H, D₂O exchanged), 2.85 (dd, 1H, *J*= 14.3, 8.5 Hz), 3.29 (dd, 1H, *J*= 14.3, 4.4 Hz), 3.40–3.50 (m, 2H), 3.64 (dd, 1H, *J*= 8.8, 4.4 Hz), 7.09 (s, 1H), 7.14 (td, 1H, *J*= 7.1, 1.1 Hz), 7.20–7.30 (m, 7H), 7.35–7.36 (m, 1H), 7.65 (d, 1H, *J*= 7.8 Hz), 8.13 (br s, 1H). ESI/MS *m/z* 332 (M-H)⁻, ESI-MS/MS *m/z* 201 (100), 130 (74).

(S)-2-Amino-3-(1H-indol-3-yl)-N-[(1-phenylcyclopropyl)methyl]propanamide ((S)-34).

Quantitative yield. ESI/MS: *m/z* 332 (M-H)⁻; ESI-MS/MS: *m/z* 201 (100); 130 (67).

(R)-2-Amino-3-(4-cyanophenyl)-N-[(1-phenylcyclopropyl)methyl]propanamide ((R)-35). 43%

Yield. ¹H NMR (CDCl₃): δ 0.87–0.97 (m, 4H), 1.72 (br s, 2H), 2.82 (dd, 1H, *J*= 14.0, 8.5 Hz), 3.21 (dd, 1H, *J*= 13.7, 4.4 Hz), 3.40 (dd, 1H, *J*= 13.9, 6.0 Hz), 3.45 (dd, 1H, *J*= 13.7, 6.0 Hz), 3.62 (dd, 1H, *J*= 8.0, 4.5 Hz), 7.19–7.24 (m, 4H), 7.27–7.31 (m, 3H), 7.58 (d, 2H, *J*= 8.2 Hz). ESI⁺/MS *m/z* 342 (M+Na)⁺, ESI⁺/MS/MS *m/z* 151(100).

(S)-2-Amino-3-(4-cyanophenyl)-N-[(1-phenylcyclopropyl)methyl]propanamide ((S)-35).

76% Yield. ESI⁺/MS *m/z* 342 (M+Na)⁺, ESI⁺/MS/MS *m/z* 151(100).

(R)-2-Amino-N-[(1-phenylcyclopropyl)methyl]-3-(3-pyridinyl)propanamide ((R)-36).

90% Yield. ¹H NMR (CDCl₃): δ 0.81–0.87 (m, 4H), 1.53 (br s, 2H), 2.71 (dd, 1H, *J*= 13.5, 8.2 Hz), 3.14 (dd, 1H, *J*= 14.1, 4.1 Hz), 3.36–3.49 (m, 2H), 3.55 (dd, 1H, *J*= 8.8, 4.1 Hz), 7.19–7.30 (m,

7H), 7.52 (d, 1H, $J=7.6$ Hz), 8.43 (d, 1H, $J=1.7$ Hz), 8.5 (dd, 1H, $J=5.3, 1.7$ Hz). ESI⁺/MS m/z 318 (M+Na)⁺, ESI⁺/MS/MS m/z 226(100).

(S)-2-Amino-N-[(1-phenylcyclopropyl)methyl]-3-(3-pyridinyl)propanamide ((S)-36).

Quantitative yield. ESI⁺/MS m/z 318 (M+Na)⁺, ESI⁺/MS/MS m/z 226 (100).

(R)-2-Amino-3-(4-cyanophenyl)-N-[[1-(4-trifluoromethoxyphenyl)cyclopropyl]methyl]propanamide ((R)-37).

92% Yield. ¹H NMR (CDCl₃): δ 0.82–0.93 (m, 4H), 1.47 (br s, 2H), 2.75 (dd, 1H, $J=13.5, 8.5$ Hz), 3.23 (dd, 1H, $J=13.5, 4.5$ Hz), 3.41 (dd, 1H, $J=14.0, 6.00$ Hz), 3.46 (dd, 1H, $J=14.0, 6.00$ Hz), 3.58 (dd, 1H, $J=8.8, 4.5$ Hz), 7.12–7.15 (m, 2H), 7.25–7.28 (m, 3H), 7.29–7.31 (m, 2H), 7.59–7.62 (m, 2H). ESI/MS: m/z 402 (M-H)⁻, ESI-MS/MS: m/z 285 (100), 116 (12).

(S)-2-Amino-3-(4-cyanophenyl)-N-[[1-(4-trifluoromethoxyphenyl)cyclopropyl]methyl]propanamide ((S)-37).

90% Yield. ESI/MS: m/z 402 (M-H)⁻, ESI-MS/MS: m/z 285 (100), 116 (13).

(R)-2-Amino-3-(4-cyanophenyl)-N-[[1-(3-fluoro-4-methylphenyl)cyclopropyl]methyl]propanamide ((R)-38).

71% Yield. ¹H NMR (CDCl₃): δ 0.76–0.82 (m, 2H), 0.83–0.88 (m, 2H), 1.47 (br s, 2H), 2.23 (s, 3H), 2.89–2.92 (m, 1H), 3.17–3.20 (m, 1H), 3.23–3.29 (m, 1H), 3.42–3.46 (m, 1H), 4.12–4.14 (m, 1H), 6.83–6.86 (m, 2H), 7.06–7.09 (m, 1H), 7.13 (br t, 1H), 7.22 (d, 2H, $J=8.5$ Hz), 7.46 (d, 2H, $J=8.5$ Hz). ESI/MS: m/z 350 (M-H)⁻, ESI-MS/MS: m/z 233 (100), 116 (67).

(S)-2-Amino-3-(4-cyanophenyl)-N-[[1-(3-fluoro-4-methylphenyl)cyclopropyl]methyl]propanamide ((S)-38)

94% yield. ESI/MS: m/z 350 (M-H)⁻, ESI-MS/MS: m/z 233 (100), 116 (61).

(R)-2-Amino-3-(4-cyanophenyl)-N-[[1-(3-chloro-4-fluorophenyl)cyclopropyl]methyl]

propanamide ((R)-39).

47% Yield. ¹H NMR (DMSO-*d*₆): δ 0.73–0.80 (m, 2H), 0.83–0.88 (m, 2H), 2.30 (br s, 2H), 2.64 (dd, 1H, *J*= 13.0, 8.0 Hz), 2.88 (dd, 1H, *J*=13.0, 5.5 Hz), 3.20 (dd, 1H, *J*= 13.0, 5.5 Hz), 3.33–3.37 (m, 1H), 3.40–3.42 (m, 1H), 7.18–7.21 (m, 1H), 7.28 (d, 1H, *J*= 9.0), 7.34 (d, 2H, *J*= 8.5 Hz), 7.38 (dd, 1H, *J*= 6.5, 2.0 Hz), 7.70 (d, 2H, *J*= 8.4 Hz), 7.91 (br t, 1H). ESI/MS: *m/z* 370 (M-H)⁻, ESI-MS/MS: *m/z* 253 (100), 116 (25).

(S)-2-Amino-3-(4-cyanophenyl)-N-[[1-(3-chloro-4-fluorophenyl)cyclopropyl]methyl]

propanamide ((S)-39).

95% Yield. ESI/MS: *m/z* 370 (M-H)⁻, ESI-MS/MS: 253 (100), 116 (21).

General Procedure for the Synthesis of the Final Compounds (Procedure A)

To a solution of the amine (*R*)- and (*S*)-**34-39** (1.0 mmol) in anhydrous THF, a solution of the appropriate 4-substituted phenylisocyanate (1.2 mmol) in the same solvent (10 mL) was added and the reaction mixture was stirred at room temperature overnight. After removing the solvent *in vacuo*, the residue was taken up in CHCl₃ (20 mL) and washed with H₂O (2 × 20 mL). The separated organic layers were dried over Na₂SO₄ and concentrated under reduced pressure. The crude residue was chromatographed (CHCl₃/AcOEt, 1:1 as the eluent). When necessary, the obtained solid was further purified by crystallization from MeOH to give the final compounds.

(R)-3-(1*H*-Indol-3-yl)-2-[3-(4-methoxyphenyl)ureido]-N-[(1-phenylcyclopropyl)methyl]

propanamide ((R)-7).

19% Yield. ¹H NMR (CDCl₃): δ 0.56–0.74 (m, 4H), 3.06 (dd, 1H, *J*= 14.6, 8.2 Hz), 3.19–3.25 (m, 3H), 3.76 (s, 3H), 4.63–4.65 (m, 1H), 5.91 (br d, 1H), 6.00 (br t, 1H), 6.73 (d, 2H, *J*= 8.8 Hz), 6.83 (d, 1H, *J*= 1.8 Hz), 6.91–6.94 (m, 3H), 7.04–7.22 (m, 7H), 7.32 (d, 1H, *J*= 8.2 Hz), 7.62 (d, 1H, *J*= 8.4 Hz), 7.97 (br s, 1H). ESI/MS: *m/z* 481 (M-H)⁻; ESI-MS/MS: *m/z* 358 (100), 332 (44).

(S)-3-(1*H*-Indol-3-yl)-2-[3-(4-methoxyphenyl)ureido]-N-[(1-phenylcyclopropyl)methyl]

propanamide ((R)-7).

22% Yield. ESI⁺/MS: *m/z* 481 (M-H)⁺; ESI-MS/MS: *m/z* 358 (100), 332 (43).

(S)-2-[3-(4-Fluorophenyl)ureido]-3-(1*H*-indol-3-yl)-*N*-[(1-phenylcyclopropyl)methyl]propanamide ((S)-8).

41% Yield. ¹H NMR (DMSO-*d*₆): δ 0.64–0.81 (m, 4H), 2.84 (dd, 1H, *J*= 14.6, 7.0 Hz), 2.99 (dd, 1H, *J*= 14.6, 5.3 Hz), 3.22 (dd, 1H, *J*= 13.5, 5.3 Hz), 3.38 (dd, 1H, *J*= 13.5, 5.8 Hz), 4.51–4.44 (m, 1H), 6.22 (br d, 1H), 6.92 (t, 2H, *J*= 7.6 Hz), 6.98–7.00 (m, 2H), 7.10–7.21 (m, 6H), 7.28–7.34 (m, 3H), 7.5 (d, 1H, *J*= 8.2 Hz), 8.02 (t, 1H, *J*= 5.3 Hz), 8.66 (s, 1H), 10.78 (s, 1H). ESI⁺/MS: *m/z* 469 (M-H)⁺, ESI-MS/MS: *m/z* 229 (6), 332 (14), 358 (100). ESI⁺/MS: *m/z* 469 (M-H)⁺; ESI-MS/MS: *m/z* 358 (100), 332 (12).

(R)-3-(1*H*-Indol-3-yl)-*N*-[(1-phenylcyclopropyl)methyl]-2-[3-(phenyl)ureido]propanamide ((R)-9).

35% Yield. ¹H NMR (CDCl₃): δ 0.49–0.74 (m, 4H), 3.09 (dd, 1H, *J*= 14.6, 8.8 Hz), 3.19–3.25 (m, 2H), 3.72–3.76 (m, 1H), 4.65–4.73 (m, 1H), 6.09 (br s, 1H), 6.40 (br t, 1H), 6.83 (br s, 1H), 6.91–6.93 (m, 2H), 6.97–7.01 (m, 1H), 7.06–7.13 (m, 4H), 7.16–7.21 (m, 5H), 7.32 (d, 1H, *J*= 8.2 Hz), 7.52 (br t, 1H), 7.65 (d, 1H, *J*= 8.2 Hz), 7.97 (s, 1H). ESI⁺/MS: *m/z* 451 (M-H)⁺; ESI-MS/MS: *m/z* 358 (100), 332 (16).

(S)-3-(1*H*-Indol-3-yl)-*N*-[(1-phenylcyclopropyl)methyl]-2-[3-(phenyl)ureido]propanamide ((S)-9).

15% Yield. ESI⁺/MS: *m/z* 451 (M-H)⁺, ESI-MS/MS: *m/z* 358 (100), 332 (10).

(R)-3-(4-Cyanophenyl)-2-[3-(4-nitrophenyl)ureido]-*N*-[(1-phenylcyclopropyl)methyl]propanamide ((R)-10).

69% Yield. ¹H NMR (DMSO-*d*₆): δ 0.69–0.84 (m, 4H), 2.79 (dd, 1H, *J*= 13.5, 7.6 Hz), 2.96 (dd, 1H, *J*= 13.5, 5.2 Hz), 3.18 (dd, 1H, *J*= 13.5, 5.3 Hz), 3.48 (dd, 1H, *J*= 14.1, 6.4 Hz), 4.51–4.58

(m, 1H), 6.61 (br d, 1H), 7.11–7.17 (m, 2H), 7.19–7.27 (m, 5H), 7.53 (d, 2H, $J = 9.1$ Hz), 7.66 (d, 2H, $J = 8.2$ Hz), 8.01 (d, 2H, $J = 8.8$ Hz), 8.22 (br t, 1H), 9.41 (br s, 1H). ESI/MS: m/z 482 (M-H)⁻, ESI-MS/MS: m/z 344 (100).

(S)-3-(4-Cyanophenyl)-2-[3-(4-nitrophenyl)ureido]-N-[(1-phenylcyclopropyl)methyl]propanamide ((S)-10).

39% Yield. ESI/MS: m/z 482 (M-H)⁻; ESI-MS/MS: m/z 344 (100).

(R)-2-[3-(4-Nitrophenyl)ureido]-N-[(1-phenylcyclopropyl)methyl]-3-(3-pyridinyl)propanamide ((R)-11).

35% Yield. ¹H NMR (DMSO-*d*₆): δ 0.73–0.85 (m, 4H), 2.73 (dd, 1H, $J = 13.5, 7.6$ Hz), 2.90 (dd, 1H, $J = 14.1, 4.7$ Hz), 3.22 (dd, 1H, $J = 14.1, 4.7$ Hz), 3.45 (dd, 1H, $J = 13.5, 5.9$ Hz), 4.51–4.53 (m, 1H), 6.65 (d, 1H, $J = 7.6$ Hz), 7.13–7.26 (m, 5H), 7.37 (m, 1H), 7.53 (d, 2H, $J = 8.9$ Hz), 8.1 (d, 2H, $J = 9.3$ Hz), 8.22–8.30 (m, 3H), 8.36 (d, 1H, $J = 4.7$ Hz), 9.45 (s, 1H). ESI/MS: m/z 458 (M-H)⁻, ESI-MS/MS: m/z 320 (100).

(S)-2-[3-(4-Nitrophenyl)ureido]-N-[(1-phenylcyclopropyl)methyl]-3-(3-pyridinyl)propanamide ((S)-11).

28% Yield. ESI/MS: m/z 458 (M-H)⁻; ESI-MS/MS: m/z 320 (100).

(R)-3-(4-Cyanophenyl)-2-[3-(4-methoxyphenyl)ureido]-N-[[1-(4-trifluoromethoxyphenyl)cyclopropyl)methyl]propanamide ((R)-12).

72% Yield. ¹H NMR (DMSO-*d*₆): δ 0.70–0.87 (m, 4H), 2.75 (dd, 1H, $J = 13.5, 8.1$ Hz), 2.92 (dd, 1H, $J = 14.1, 5.1$ Hz), 3.19 (dd, 1H, $J = 14.1, 5.1$ Hz), 3.42 (dd, 1H, $J = 14.1, 6.0$ Hz), 3.66 (s, 3H), 4.46–4.53 (m, 1H), 6.20 (br d, 1H), 6.78 (d, 2H, $J = 8.7$ Hz), 7.17–7.21 (m, 4H), 7.26 (d, 2H, $J = 8.4$ Hz), 7.36 (d, 2H, $J = 8.7$ Hz), 7.68 (d, 2H, $J = 8.1$ Hz), 8.16 (br t, 1H), 8.39 (s, 1H). ESI-MS: m/z 551 (M-H)⁻, ESI-MS/MS: m/z 428 (46), 402 (23), 385 (100).

(S)-3-(4-Cyanophenyl)-2-[3-(4-methoxyphenyl)ureido]-N-[[1-(4-

trifluoromethoxyphenyl)cyclopropyl)methyl]propanamide ((S)-12).

76% Yield. ESI-MS: m/z 551 (M-H)⁻, ESI-MS/MS: m/z 428 (50), 385 (100).

(R)-3-(4-Cyanophenyl)-2-[3-(4-fluorophenyl)ureido]-N-[[1-(4-trifluoromethoxyphenyl)cyclopropyl)methyl]propanamide ((R)-13).

64% Yield. ¹H NMR (DMSO-*d*₆): δ 0.72–0.74 (m, 2H), 0.80–0.82 (m, 2H), 2.76 (dd, 1H *J*= 13.5, 8.5 Hz), 2.92 (dd, 1H, *J*= 13.5, 5.5 Hz), 3.20 (dd, 1H, *J*= 13.5, 5.5 Hz), 3.44 (dd, 1H, *J*= 14.0, 6.5 Hz), 4.49–4.53 (m, 1H), 6.32 (br d, 1H), 7.01–7.05 (m, 2H), 7.20 (d, 2H, *J*= 8.5 Hz), 7.25 (d, 2H, *J*= 8.5 Hz), 7.29–7.34 (m, 2H), 7.35–7.38 (m, 2H), 7.69 (d, 2H, *J*= 8.5 Hz), 8.24 (br t, 1H), 8.65 (s, 1H). ESI/MS: m/z 539 (M-H)⁻, ESI-MS/MS: m/z 428 (94), 385 (100).

(S)-3-(4-Cyanophenyl)-2-[3-(4-fluorophenyl)ureido]-N-[[1-(4-trifluoromethoxyphenyl)cyclopropyl)methyl]propanamide ((R)-13).

80% Yield. ESI/MS: m/z 539 (M-H)⁻, ESI-MS/MS: m/z 428 (86), 385 (100).

(R)-N-[[1-(3-Chloro-4-fluorophenyl)cyclopropyl)methyl]-3-(4-cyanophenyl)-2-[3-(4-methoxyphenyl)ureido]propanamide ((R)-16).

19% Yield. ¹H NMR (DMSO-*d*₆): δ 0.72–0.87 (m, 4H), 2.76 (dd, 1H, *J*= 13.5, 7.5 Hz), 2.92 (dd, 1H, *J*= 13.5, 5.5 Hz), 3.14 (dd, 1H, *J*= 14.0, 5.0 Hz), 3.44 (dd, 1H, *J*= 14.0, 6.5 Hz), 3.67 (s, 3H), 4.50 (td, 1H, *J*= 8.5, 6.0 Hz), 6.25 (br d, 1H), 6.78 (d, 2H, *J*= 9.0 Hz), 7.19–7.22 (m, 2H), 7.24–7.27 (m, 4H), 7.45 (d, 1H, *J*= 7.5 Hz), 7.69 (d, 2H, *J*= 8.5 Hz), 8.22 (br t, 1H), 8.42 (s, 1H). ESI-MS: m/z 519 (M-H)⁻, ESI-MS/MS: m/z 396 (50), 370 (30), 353 (100).

(S)-N-[[1-(3-Chloro-4-fluorophenyl)cyclopropyl)methyl]-3-(4-cyanophenyl)-2-[3-(4-methoxyphenyl)ureido]propanamide ((S)-16).

50% Yield. ESI-MS: m/z 519 (M-H)⁻, ESI-MS/MS: m/z 396 (50), 370 (32), 353 (100).

(R)-3-(4-Cyanophenyl)-N-[[1-(3-fluoro-4-methylphenyl)cyclopropyl)methyl]-2-[3-(4-

methoxyphenyl)ureido]propanamide ((R)-14).

13% Yield. ¹H NMR (DMSO-*d*₆): δ 0.74–0.78 (m, 2H), 0.81–0.86 (m, 2H), 2.14 (s, 3H), 2.78 (dd, 1H, *J*= 14.0, 8.0 Hz), 2.94 (dd, 1H, *J*= 14.0, 5.5 Hz), 3.18 (dd, 1H, *J*= 14.0, 5.5 Hz), 3.44 (dd, 1H, *J*= 14.0, 6.5 Hz), 3.67 (s, 3H), 4.48–4.52 (m, 1H), 6.26 (br d, 1H), 6.78 (d, 2H, *J*= 8.8 Hz), 6.95–6.98 (m, 1H), 7.02 (d, 1H, *J*= 1.5 Hz), 7.12 (t, 1H, *J*= 8.0 Hz), 7.21 (d, 2H, *J*= 8.8 Hz), 7.26 (d, 2H, *J*= 8.3 Hz), 7.67 (d, 2H, *J*= 8.5 Hz), 8.18 (br t, 1H), 8.46 (s, 1H). ESI[−]/MS: *m/z* 499 (M-H)[−], ESI[−]-MS/MS: *m/z* 376 (42), 333 (100).

(R)-3-(4-Cyanophenyl)-N-[[1-(3-fluoro-4-methylphenyl)cyclopropyl]methyl]-2-[3-(4-fluorophenyl)ureido]propanamide ((R)-15).

10% Yield. ¹H NMR (DMSO-*d*₆): δ 0.71–0.86 (m, 4H), 2.14 (s, 3H), 2.79 (dd, 1H, *J*= 13.7, 7.8 Hz), 2.94 (dd, 1H, *J*= 13.7, 5.4 Hz), 3.19 (dd, 1H, *J*= 14.2, 5.0 Hz), 3.44 (dd, 1H, *J*= 14.2, 6.4 Hz), 4.51–4.52 (m, 1H), 6.36 (br d, 1H), 6.96 (td, 2H, *J*= 8.5, 1.5 Hz), 7.01–7.05 (m, 2H), 7.12 (t, 1H, *J*= 8.0 Hz), 7.25 (d, 2H, *J*= 7.8 Hz), 7.30–7.35 (m, 2H), 7.67 (d, 2H, *J*= 8.5 Hz), 8.19 (br t, 1H), 8.70 (s, 1H). ESI[−]/MS: *m/z* 487 (M-H)[−], ESI[−]-MS/MS: *m/z* 376 (75), 333 (100).

(S)- 3-(4-Cyanophenyl)-N-[[1-(3-chloro-4-fluorophenyl)cyclopropyl]methyl]-2-[3-(4-fluorophenyl)ureido]propanamide ((S)-17).

34% Yield. ¹H NMR (DMSO-*d*₆): δ 0.73–0.89 (m, 4H), 2.77 (dd, 1H, *J*= 13.7, 7.8 Hz), 2.93 (dd, 1H, *J*= 13.7, 5.3 Hz), 3.15 (dd, 1H, *J*= 14.2, 5.4 Hz), 3.44 (dd, 1H, *J*= 14.2, 7 Hz), 4.48–4.53 (m, 1H), 6.30 (br d, 1H), 7.01–7.06 (m, 2H), 7.25 (t, 2H, *J*= 7.8 Hz), 7.29–7.33 (m, 4H), 7.45 (dt, 1H, *J*= 6.0, 2.0 Hz), 7.69 (d, 2H, *J*= 6.4 Hz), 8.24 (br t, 1H), 8.63 (s, 1H). ESI[−]/MS: *m/z* 507 (M-H)[−], ESI[−]-MS/MS: *m/z* 396 (100), 353 (89).

General Procedure for the Synthesis of the Final Compounds (Procedure B)

N,N'-Carbonyldiimidazole (1.1 mmol) was added to a solution of aniline (1.0 mmol), in anhydrous

THF (10 mL), under N₂. The reaction mixture was stirred at room temperature overnight, then a solution of the amine (*R*)-**34**, (*S*)-**38**, or (*S*)-**39**, (1.0 mmol) in anhydrous THF was added. The reaction mixture was stirred until the reagents disappeared monitoring by TLC. Then, the solvent was removed *in vacuo* and the residue was partitioned between EtOAc (20 mL) and H₂O (20 mL). The separated aqueous layer was extracted twice with EtOAc (20 mL), then the collected organic layers were dried (Na₂SO₄) and evaporated *in vacuo*. The crude residue was chromatographed to give pure target compound as a white solid. When necessary, the obtained solid was further purified by crystallization from MeOH to give the final compound.

(*R*)-2-[3-(4-Fluorophenyl)ureido]-3-(1*H*-indol-3-yl)-*N*-[(1-phenylcyclopropyl)methyl]propanamide ((*R*)-8**).**

19% Yield. ¹H NMR (DMSO-*d*₆): δ 0.65–0.80 (m, 4H), 2.84 (dd, 1H, *J*= 14.6, 7.0 Hz), 2.99 (dd, 1H, *J*= 14.6, 5.3 Hz), 3.22 (dd, 1H, *J*= 13.5, 5.3 Hz), 3.38 (dd, 1H, *J*= 13.5, 5.8 Hz), 4.51–4.44 (m, 1H), 6.22 (br d, 1H), 6.92 (t, 2H, *J*= 7.6 Hz), 6.98–7.00 (m, 2H), 7.10–7.21 (m, 6H), 7.28–7.34 (m, 3H), 7.5 (d, 1H, *J*= 8.2 Hz), 8.02 (t, 1H, *J*= 5.3 Hz), 8.66 (s, 1H), 10.78 (s, 1H). ESI⁺/MS: *m/z* 469 (M-H)⁺, ESI⁻-MS/MS: *m/z* 229 (6), 332 (14), 358 (100).

(*S*)-3-(4-Cyanophenyl)-*N*-[[1-(3-fluoro-4-methylphenyl)cyclopropyl]methyl]-2-[3-(4-methoxyphenyl)ureido]propanamide ((*S*)-14**).**

13% Yield. ¹H NMR (DMSO-*d*₆): δ 0.74–0.78 (m, 2H), 0.81–0.86 (m, 2H), 2.14 (s, 3H), 2.78 (dd, 1H, *J*= 14.0, 8.0 Hz), 2.94 (dd, 1H, *J*= 14.0, 5.5 Hz), 3.18 (dd, 1H, *J*= 14.0, 5.5 Hz), 3.44 (dd, 1H, *J*= 14.0, 6.5 Hz), 3.67 (s, 3H), 4.48–4.52 (m, 1H), 6.26 (br d, 1H), 6.78 (d, 2H, *J*= 8.8 Hz), 6.95–6.98 (m, 1H), 7.02 (d, 1H, *J*= 1.5 Hz), 7.12 (t, 1H, *J*= 8.0 Hz), 7.21 (d, 2H, *J*= 8.8 Hz), 7.26 (d, 2H, *J*= 8.3 Hz), 7.67 (d, 2H, *J*= 8.5 Hz), 8.18 (br t, 1H), 8.46 (s, 1H). ESI⁺/MS: *m/z* 499 (M-H)⁺, ESI⁻-MS/MS: *m/z* 376 (39), 333 (100).

(S)-3-(4-Cyanophenyl)-2-[3-(4-fluorophenyl)ureido]-N-[[1-(3-fluoro-4-methylphenyl)cyclopropyl]methyl]propanamide ((S)-15).

10% Yield. ¹H NMR (DMSO-*d*₆): δ 0.71–0.86 (m, 4H), 2.14 (s, 3H), 2.79 (dd, 1H, *J*= 13.7, 7.8 Hz), 2.94 (dd, 1H, *J*= 13.7, 5.4 Hz), 3.19 (dd, 1H, *J*= 14.2, 5.0 Hz), 3.44 (dd, 1H, *J*= 14.2, 6.4 Hz), 4.51–4.52 (m, 1H), 6.36 (br d, 1H), 6.96 (td, 2H, *J*= 8.5, 1.5 Hz), 7.01–7.05 (m, 2H), 7.12 (t, 1H, *J*= 8.0 Hz), 7.25 (d, 2H, *J*= 7.8 Hz), 7.30–7.35 (m, 2H), 7.67 (d, 2H, *J*= 8.5 Hz), 8.19 (br t, 1H), 8.70 (s, 1H). ESI/MS: *m/z* 487 (M-H)⁻, ESI-MS/MS: *m/z* 376 (77), 333 (100).

(R)-3-(4-Cyanophenyl)-N-[[1-(3-chloro-4-fluorophenyl)cyclopropyl]methyl]-2-[3-(4-fluorophenyl)ureido]propanamide ((R)-17).

15% Yield. ¹H NMR (DMSO-*d*₆): δ 0.73–0.89 (m, 4H), 2.77 (dd, 1H, *J*= 13.7, 7.8 Hz), 2.93 (dd, 1H, *J*= 13.7, 5.3 Hz), 3.15 (dd, 1H, *J*= 14.2, 5.4 Hz), 3.44 (dd, 1H, *J*= 14.2, 7 Hz), 4.48–4.53 (m, 1H), 6.30 (br d, 1H), 7.01–7.06 (m, 2H), 7.25 (t, 2H, *J*= 7.8 Hz), 7.29–7.33 (m, 4H), 7.45 (dt, 1H, *J*= 6.0, 2.0 Hz), 7.69 (d, 2H, *J*= 6.4 Hz), 8.24 (br t, 1H), 8.63 (s, 1H). ESI/MS: *m/z* 507 (M-H)⁻, ESI-MS/MS: *m/z* 396 (92), 353 (100).

Stability Assays in Rat Liver Microsomes. Test compounds were pre-incubated at 37 °C with rat liver microsomes (Tebu-Bio, Milan, Italy) (1.0 mg/mL microsomal protein) at 10 μM final concentration in 100 mM potassium phosphate buffer (pH 7.4) for 10 min. Metabolic reactions were initiated by the addition of the NADPH regenerating system (containing 10 mM NADP, 50 mM glucose-6-phosphate, and 10 unit/mL glucose-6-phosphate dehydrogenase, final glucose-6-phosphate dehydrogenase concentration, 1 unit/mL). Aliquots were removed at specific time endpoints (0, 5, 15, 30 and 60 min) and immediately mixed with an equal volume of cold acetonitrile containing the internal standard. Test compound incubated with microsomes without NADPH regenerating system was included. Quenched samples were centrifuged at 4500 rpm for 15 min and the supernatants were injected for quantification analysis. Samples (100 μL) were analyzed

by using an Agilent 1260 Infinity Binary LC System equipped with a diode array detector (Open Lab software was used to analyze the chromatographic data) and a Phenomenex Gemini C-18 column (250 × 4.6 mm, 5 μm particle size). The samples were eluted using CH₃CN/20 mM ammonium formate pH 5.5 (70:30, v/v) as eluent (1 mL/min). Concentrations were quantified by measuring the area under the peak.

The percentage of the parent compound remaining after a 30-min incubation has been calculated according to the equation:

$$\% \text{ of parent compound remaining after 30 min} = C_{\text{parent}}/C_{\text{control}} \times 100$$

where C_{parent} is ligand concentration after incubation with microsome fraction and NADPH regenerating system and C_{control} is ligand concentration after incubation with microsome fraction only.

The *in vitro* half life ($t_{1/2}$) was calculated using the expression $t_{1/2}=0.693/b$, where b is the slope found in the linear fit of the natural logarithm of the fraction remaining of the parent compound vs incubation time.⁵³ *In vitro* half-life was then used to calculate the intrinsic plasma clearance (CL_{int}) according to the following equation:

$$CL_{\text{int}}: \frac{0.693}{\text{In vitro } t_{1/2}} \text{ ¥ } \frac{1}{\text{mg/ml microsomal protein}}$$

2. Biological methods.

Ca²⁺ Mobilization Assay in HL-60 transfected cells and human neutrophils.

Cell Culture. Human promyelocytic leukemia HL-60 cells stably transfected with FPR1 (FPR1-HL-60 cells) or FPR2 (FPR2-HL-60 cells) (kind gifts from Dr. Marie-Joséphine Rabiet, INSERM, Grenoble, France) were cultured in RPMI 1640 medium supplemented with 10% heat-inactivated fetal calf serum, 10 mM HEPES, 100 μg/ml streptomycin, 100 U/ml penicillin, and G418 (1 mg/mL), as described previously.³² Wild-type HL-60 cells were cultured under the same conditions, but without G418.

Isolation of Human Neutrophils. Blood was collected from healthy donors in accordance with a protocol approved by the Institutional Review Board at Montana State University. Neutrophils were purified from the blood using dextran sedimentation, followed by Histopaque 1077 gradient separation and hypotonic lysis of red blood cells, as previously described (Schepetkin 2007).⁵⁴ Isolated neutrophils were washed twice and resuspended in HBSS without Ca^{2+} and Mg^{2+} (HBSS^-). Neutrophil preparations were routinely >95% pure, as determined by light microscopy, and >98% viable, as determined by trypan blue exclusion.

Ca²⁺ Mobilization Assay. Changes in intracellular Ca^{2+} were measured with a FlexStation II scanning fluorometer (Molecular Devices, Sunnyvale, CA) for human neutrophils and HL-60 cells, as described previously.³² All active compounds were evaluated in parent (wild-type) HL-60 cells for supporting that the agonists are inactive in non-transfected cells. Human neutrophils or HL-60 cells, suspended in HBSS^- containing 10 mM HEPES, were loaded with Fluo-4 AM dye (Invitrogen) (1.25 $\mu\text{g}/\text{mL}$ final concentration) and incubated for 30 min in the dark at 37 °C. After dye loading, the cells were washed with HBSS^- containing 10 mM HEPES, resuspended in HBSS containing 10 mM HEPES and Ca^{2+} and Mg^{2+} (HBSS^+), and aliquotted into the wells of a flat-bottomed, half-area-well black microtiter plates (2×10^5 cells/well). If indicated, 2 mM probenecid was added 5 min before the assay. The compound of interest was added from a source plate containing dilutions of test compounds in HBSS^+ , and changes in fluorescence were monitored ($\lambda_{\text{ex}} = 485$ nm, $\lambda_{\text{em}} = 538$ nm) every 5 s for 240 s at room temperature after automated addition of compounds. Maximum change in fluorescence, expressed in arbitrary units over baseline, was used to determine agonist response. Responses were normalized to the response induced by 5 nM fMLF for FPR1-HL-60 cells and neutrophils, or 5 nM WKYMVM for FPR2-HL-60 cells, which were assigned a value of 100%. Curve fitting (5–6 points) and calculation of median effective

concentration values (EC_{50}) were performed by nonlinear regression analysis of the dose–response curves generated using Prism 5 (GraphPad Software Inc., San Diego, CA).

Evaluation of anti-inflammatory properties in rat primary microglial cell cultures.

Cell culture. Primary cultures of microglial cells were prepared from cortices of 1–2-day-old Sprague-Dawley rat pups as previously described.³ Briefly, after decapitation, brains were removed immediately, and cerebral cortices were cut into small pieces. The minced tissue was incubated in dissecting medium HBSS (Gibco, USA) containing glucose, BSA and HEPES with 0.025% trypsin at 37 °C for 20 min. The trypsinization process was stopped by adding trypsin inhibitor from Glycine max (soybean) (Sigma-Aldrich, USA). A completely dissociated suspension of the tissue was prepared by mild trituration. Next, cells were plated at the density of 3×10^5 cells/cm² in culture medium consisting of DMEM with GlutaMax and high glucose (4.5 g/L) supplemented with heat-inactivated 10% FBS, 100 U/mL penicillin, and 0.1 mg/mL streptomycin on poly-L-lysine-coated 75-cm² culture flasks. After 3 days, culture medium was removed and replaced with fresh medium. On the 9th day *in vitro* (37 °C, 95% O₂/5% CO₂), flasks were agitated on a horizontal shaker. After centrifugation, cells were resuspended in culture medium, and cell viability was determined by trypan blue exclusion. The cells were plated at a final density of 2×10^5 cells/well in 24-well plates or 4×10^4 cells/well in 96-well plates. The purity of microglial cell cultures was assessed using an anti-Iba-1 antibody and anti-CD11b antibody. More than 95% of cells were stained positively. Two days after plating, the cells were used for experiments.

Cell treatment. In all experiments, cells were pre-treated for 1 h with various concentrations of FPR2 agonists (*S*)-**10**, (*R*)-**11** and (*S*)-**17** and then stimulated for 24 hours with the lipopolysaccharide (LPS; 100 ng/ml) (*Escherichia coli* 0111:B4, Sigma-Aldrich, USA). Control (un-stimulated) cells were treated with vehicle. Additionally, in experiments where the secretion of NO or cytokines were measured, the FPR2 antagonist WRW4 (Alomone Labs, Israel) was added 30

min before agonists (Figure 6).

Cell viability test. Cell viability was determined by the tetrazolium salt 3-[4,5-dimethylthiazol-2-yl]-2,5-diphenyltetrazolium bromide (MTT) (Sigma Aldrich, Germany) assay. Microglial cells were seeded into 96-well plates at a density of 4×10^4 per well, with 100 μ L of culture medium, and incubated for 48 h to allow cell adherence. At 24 h after treatment with different concentrations of tested compounds, MTT (at 0.15 mg/mL) was added to each well and incubated for 2 h at 37 °C. Next, culture medium was discarded, and 0.1 M HCl in isopropanol was added to dissolve the formazan dye. The absorbance value was measured using a multiwell spectrophotometer Infinite® 200 PRO Detector (TECAN, Switzerland) at 570 nm. The data were normalized to the absorbance in the vehicle-treated cells (100%) and expressed as a percentage of the control \pm SEM.

Lactate dehydrogenase (LDH) test. To quantify the cell death, the level of lactate dehydrogenase release from the damaged cells into the culture media was measured 24 h after treatment. Cell culture supernatants were collected from each well of the 96-well plates and were incubated with the appropriate reagent mixture according to the supplier's instructions (Cytotoxicity Detection Kit, Roche, Germany) at room temperature for 20 min. In this test, the amount of formazan salt, formed after the conversion of lactate to pyruvate and then by reduction of tetrazolium salt, is proportional to the LDH activity in the sample. The intensity of the red color formed in the assay, measured at a wavelength of 490 nm (Infinite® 200 PRO Detector, TECAN, Switzerland) is proportional to LDH activity and also to the number of damaged cells. The data were normalized to the activity of LDH released from vehicle-treated cells (100%) and expressed as a percentage of the control \pm SEM.

NO release assay. Nitric oxide (NO) secreted in microglial culture medium was measured by a Griess reaction. After 24 h of treatment of microglia, 50 μ L of supernatant was collected and mixed with an equal volume of Griess reagent (0.1% *N*-1-naphthylethylenediamine dihydrochloride and

1% sulfanilamide in 5% phosphoric acid) in a 96-well plate and incubated for 10 min at room temperature. Absorbance was measured at 540 nm in a microplate reader (Infinite® 200 PRO Detector, TECAN, Switzerland). The data were normalized to the NO released from vehicle-treated cells (100%) and expressed as a percentage of the control \pm SEM.

Enzyme-linked immunosorbent assay (ELISA). The medium of microglial cells for TNF- α and IL-1 β was collected at 24 h after treatment. The protein levels of the cytokines TNF- α , IL-1 β , (R&D Systems, USA) in the culture medium were measured using commercially available enzyme-linked immunosorbent assay kits according to the manufacturers' instructions. The detection limits were as follows: TNF- α , 5 pg/ml; IL-1 β , 5 pg/ml. Inter-assay precision were as follows: TNF- α : <8.8%; IL-1 β <4.4%; intra-assay precision: TNF- α : <2.1%; IL-1 β : <3.9%.

Evaluation of permeability in hCMEC/D3 cells.

Cell cultures. hCMEC/D3 cells, a primary human brain microvascular endothelial stabilized cell line, were a kind gift from Prof. Pierre-Olivier Couraud (Institut Cochin, Centre National de la Recherche Scientifique UMR 8104, INSERM U567, Paris, France) and were cultured according to Weksler et al.⁴⁹ Cells were seeded at 50,000/cm² density, and grown for 7 days up to confluence in Transwell devices (0.4 μ m diameter pores-size, Corning Life Sciences, Chorges, France), to allow the formation of a competent BBB. Before each experiment, the transendothelial electrochemical resistance (TEER) and the permeability coefficients of dextran- fluorescein isothiocyanate (FITC), [¹⁴C]-sucrose, and [¹⁴C]-inulin were measured and taken as parameters of paracellular transport across hCMEC/D3 monolayer.⁵⁵ The TEER value was between 29 and 40 Ω cm², the dextran-FITC permeability coefficient was $0.017 \pm 0.005 \times 10^{-3}$ cm min⁻¹, the [¹⁴C]-sucrose permeability coefficient was $1.17 \pm 0.08 \times 10^{-3}$ cm min⁻¹, the [¹⁴C]-inulin permeability coefficient was $0.37 \pm 0.08 \times 10^{-3}$ cm min⁻¹. These values supported the functional integrity of the BBB monolayer.⁴⁵

Permeability of compounds through hCMEC/D3 cell monolayer. hCMEC/D3 cells, seeded as reported above in Transwell devices, were incubated at day 7 with free medium, then washed and rinsed with sterile PBS for 2 h at 37°C. 100 µM compounds were added in the upper or lower chamber for 2 h. After this incubation time, the medium in each chamber was collected and the amount of compound recovered was measured spectrophotometrically ($\lambda = 230$ nm) using a Synergy HTX Multi-Mode Reader (Bio-Tek Instruments, Winooski, VT).

Standard calibration curves were prepared at maximum absorption wavelength of each compound using PBS as solvent and were linear ($r^2 = 0.999$) over the range of tested concentration (from 5 to 10 µM). Each compound was tested in triplicate, and the experiments were repeated three times. Data are reported as the apparent permeability (P_{app}), in units of nm/s, determined as indicated in the following equation:

$$P_{app} = \frac{V_a}{\text{Area} \times \text{time}} \times \frac{[\text{drug}]_{\text{acceptor}}}{[\text{drug}]_{\text{donor}}}$$

where V_a is the volume in the acceptor well, Area is the surface area of the membrane and time is the total transport time, $[\text{drug}]_{\text{acceptor}}$ is the concentration of the drug measured by UV-spectroscopy, and $[\text{drug}]_{\text{initial}}$ is the initial drug concentration in the AP or BL chamber.

Efflux ratio (ER) was calculated using the following equation: $ER = P_{app, BA} / P_{app, AB}$, where $P_{app, BA}$ is the apparent permeability of basal-to-apical transport, and $P_{app, AB}$ is the apparent permeability of apical-to-basal transport.

References

1. Graeber, M. B.; Streit, W. J. Microglia: biology and pathology. *Acta Neuropathol.* **2010**, *119*, 89–105.
2. Amor, S.; Puentes, F.; Baker, D.; van der Valk, P. Inflammation in neurodegenerative diseases. *Immunology* **2010**, *129*, 154–169.
3. Ślusarczyk, J.; Trojan, E.; Głombik, K.; Budziszewska, B.; Kubera, M.; Lasoń, W.; Popiołek-Barczyk, K.; Mika, J.; Wędzony, K.; Basta-Kaim A. Prenatal stress is a vulnerability factor for altered morphology and biological activity of microglia cells. *Front Cell Neurosci.* **2015**, *12*, 9:82.
4. DiSabato, D. J.; Quan, N.; Godbout, J. P. Neuroinflammation: the devil is in the details. *J. Neurochem.* **2016**, *139*, 136–153.
5. Pocock, J. M.; Kettenmann H. Neurotransmitter receptors on microglia. *Trends Neurosci.* **2007**, *30*, 527–535.
6. Lucin, K. M.; Wyss-Coray, T. Immune activation in brain aging and neurodegeneration: too much or too little? *Neuron* **2009**, *64*, 110–122.
7. Serhan, C. N.; Brain, S. D.; Buckley, C. D.; Gilroy, D. W.; Haslett, C.; O'Neill, L. A.; Perretti, M.; Rossi, A. G.; Wallace, J. L. Resolution of inflammation: state of the art, definitions and terms. *FASEB J.* **2007**, *21*, 325–332.
8. Chiang, N.; Serhan, C. N.; Dahlén, S. E.; Drazen, J. M.; Hay, D. W.; Rovati, G. E.; Shimizu, T.; Yokomizo, T.; Brink, C. The lipoxin receptor ALX: Potent ligand-specific and stereoselective actions in vivo. *Pharmacol. Rev.* **2006**, *58*, 463–487.
9. Ye, R. D.; Boulay, F.; Wang, J. M.; Dahlgren, C.; Gerard, C.; Parmentier, M.; Serhan, C. N.; Murphy, P. M. International Union of Basic and Clinical Pharmacology: LXXIII. Nomenclature for the formyl peptide receptor (FPR) family. *Pharmacol. Rev.* **2009**, *61*, 119–161.
10. Lacy, M.; Jones, J.; Whittemore, S. R.; Haviland, D. L.; Wetsel, R. A.; Barnum, S. R. Expression of the receptors for the C5a anaphylatoxin, interleukin-8 and FMLP by human astrocytes and microglia. *J. Neuroimmunol.* **1995**, *61*, 71–78.

11. Cui, Y.; Le, Y.; Yazawa, H.; Gong, W.; Wang, J. M. Potential role of the formyl peptide receptor-like 1 (FPRL1) in inflammatory aspects of Alzheimer's disease. *J. Leukoc. Biol.* **2002**, *72*, 628–635.
12. Svensson, C. I.; Zattoni, M.; Serhan, C. N. Lipoxins and aspirin-triggered lipoxin inhibit inflammatory pain processing. *J. Exp. Med.* **2007**, *204*, 245–252.
13. Zhu, G.; Tang, W.; Wang, L.; Wang, C.; Wang, X. Identification of a uniquely expanded V1R (ORA) gene family in the Japanese grenadier anchovy (*Coilia nasus*). *Mar. Biol.* **2016**, *163*, 126.
14. Bufe, B.; Schumann, T.; Zufall, F. Formyl peptide receptors from immune and vomeronasal system exhibit distinct agonist properties. *J. Biol. Chem.* **2012**, *287*, 33644–33655.
15. Pei, L.; Zhang, J.; Zhao, F.; Su, T.; Wei, H.; Tian, J.; Li, M.; Shi, J. Annexin 1 exerts anti-nociceptive effects after peripheral inflammatory pain through formyl-peptide-receptor-like 1 in rat dorsal root ganglion. *Br. J. Anaesth.* **2011**, *107*, 948–958.
16. Wang, G.; Zhang, L.; Chen, X.; Xue, X.; Guo, Q.; Liu, M.; Zhao, J. Formylpeptide Receptors Promote the Migration and Differentiation of Rat Neural Stem Cells. *Sci. Rep.* **2016**, *6*, 25946.
17. Fiore, S.; Maddox, J. F.; Perez, H. D.; Serhan, C. N. Identification of a human cDNA encoding a functional high affinity lipoxin A4 receptor. *J. Exp. Med.* **1994**, *180*, 253–260.
18. Cooray, S. N.; Thomas Gobbetti, T.; Montero-Melendez, T.; McArthur, S.; Thompson, D.; Clark, A. J. L.; Flower, R.J.; Perretti, M. Ligand-specific conformational change of the G-protein-coupled receptor ALX/FPR2 determines proresolving functional responses. *Proc. Natl. Acad. Sci.* **2013**, *110*, 18232–18237.
19. Devchand, P. R.; Arita, M.; Hong, S.; Bannenberg, G.; Moussignac, R. L.; Gronert, K.; Serhan, C. N. Human ALX receptor regulates neutrophil recruitment in transgenic mice: roles in inflammation and host defense. *FASEB J.* **2003**, *17*, 652–659.
20. Sordi, R.; Menezes-de-Lima, O.; Horewicz, V.; Scheschowitsch, K., Santos, L. F., Assreuy, J. Dual role of lipoxin A4 in pneumosepsis pathogenesis. *Int. Immunopharmacol.* **2013**, *2*, 283–292.
21. Dufton, N.; Hannon, R.; Brancaleone, V.; Dalli, J.; Patel, H. B.; Gray, M.; D'Acquisto, F.;

- Buckingham, J. C.; Perretti, M.; Flower, R. J. Anti-inflammatory role of the murine formyl-peptide receptor 2: ligand-specific effects on leukocyte responses and experimental inflammation. *J. Immunol.* **2010**, *184*, 2611–2619.
22. Perretti, M.; Leroy, X.; Bland, E. J.; Montero-Melendez T. Resolution pharmacology: opportunities for therapeutic innovation in inflammation. *Trends Pharmacol. Sci.* **2015**, *36*, 737–755.
23. Romano, M.; Cianci, E.; Simiele, F.; Recchiuti, A. Lipoxins and aspirin-triggered lipoxins in resolution of inflammation. *Eur. J. Pharmacol.* **2015**, *760*, 49–63.
24. Martini, A. C.; Berta, T.; Forner, S.; Chen, G.; Bento, A. F.; Ji, R. R.; Rae, G. A. Lipoxin A4 inhibits microglial activation and reduces neuroinflammation and neuropathic pain after spinal cord hemisection. *J. Neuroinflammation.* **2016**, *13*, 75.
25. Guo, Z.; Hu, Q.; Xu, L.; Guo, Z. N.; Ou, Y.; He, Y.; Yin, C.; Sun, X.; Tang, J.; Zhang, J. H. Lipoxin A4 Reduces Inflammation Through Formyl Peptide Receptor 2/p38 MAPK Signaling Pathway in Subarachnoid Hemorrhage Rats. *Stroke.* **2016**, *47*, 490–497.
26. Medeiros, R.; Kitazawa, M.; Passos, G. F.; Baglietto-Vargas, D.; Cheng, D.; Cribbs, D. H.; LaFerla, F. M. Aspirin-triggered lipoxin A4 stimulates alternative activation of microglia and reduces Alzheimer disease-like pathology in mice. *Am. J. Pathol.* **2013**, *182*, 1780–1789.
27. Corminboeuf, O.; Leroy, X. FPR/ALXR agonists and the resolution of inflammation. *J. Med. Chem.* **2015**, *58*, 537–559.
28. Frohn, M.; Xu, H.; Zou, X.; Chang, C.; McElvaine, M.; Plant, M. H.; Wong, M.; Tagari, P.; Hungate, R.; Burli, R. W. New ‘chemical probes’ to examine the role of the hFPR1 (or ALXR) receptor in inflammation. *Bioorg. Med. Chem. Lett.* **2007**, *17*, 6633–6637.
29. Forsman, H.; Kalderen, C.; Nordin, A.; Nordling, E.; Jensen, A. J.; Dahlgren, C. Stable formyl peptide receptor agonists that activate the neutrophil NADPH-oxidase identified through screening of a compound library. *Biochem. Pharmacol.* **2011**, *81*, 402–411.

30. He, M.; Cheng, N.; Gao, W. W.; Zhang, M.; Zhang, Y. Y.; Ye, R. D.; Wang, M. W. Characterization of Quin-C1 for its anti-inflammatory property in a mouse model of bleomycin-induced lung injury. *Acta Pharmacol. Sin.* **2011**, *32*, 601–610.
31. Burli, R. W.; Xu, H.; Zou, X.; Muller, K.; Golden, J.; Frohn, M.; Adlam, M.; Plant, M. H.; Wong, M.; McElvain, M.; Regal, K.; Viswanadhan, V. N.; Tagari, P.; Hungate, R. Potent hFPRL1 (ALXR) agonists as potential anti-inflammatory agents. *Bioorg. Med. Chem. Lett.* **2006**, *16*, 3713–3718.
32. Schepetkin, I. A.; Kirpotina, L. N.; Khlebnikov, A. I.; Leopoldo, M.; Lucente, E.; Lacivita, E.; De Giorgio, P.; Quinn, M. T. 3-(1*H*-Indol-3-yl)-2-[3-(4-nitrophenyl)ureido]propanamide enantiomers with human formyl-peptide receptor agonist activity: molecular modeling of chiral recognition by FPR2. *Biochem. Pharmacol.* **2013**, *85*, 404–416.
33. Lacivita, E.; Schepetkin, I. A.; Stama, M. L.; Kirpotina, L. N.; Colabufo, N. A.; Perrone, R.; Khlebnikov, A. I.; Quinn, M. T.; Leopoldo, M. Novel 3-(1*H*-indol-3-yl)-2-[3-(4-methoxyphenyl)ureido]propanamides as Selective Agonists of Human Formyl-Peptide Receptor 2. *Bioorg. Med. Chem.* **2015**, *23*, 3913–3924.
34. He, H. Q.; Liao, D.; Wang, Z. G.; Wang, Z. L.; Zhou, H. C.; Wang, M. W.; Ye, R. D. Functional characterization of three mouse formyl peptide receptors. *Mol. Pharmacol.* **2013**, *83*, 389–398.
35. Kao, W.; Gu, R.; Jia, Y.; Wei, X.; Fan, H.; Harris, J.; Zhang, Z.; Quinn, J.; Morand, E. F.; Yang, Y. H. A formyl peptide receptor agonist suppresses inflammation and bone damage in arthritis. *Br. J. Pharmacol.* **2014**, *171*, 4087–4096.
36. Lacivita, E.; Podlewska, S.; Speranza, L.; Niso, M.; Satała, G.; Perrone, R.; Perrone-Capano, C.; Bojarski, A. J.; Leopoldo, M. Structural modifications of the serotonin 5-HT₇ receptor agonist N-(4-cyanophenylmethyl)-4-(2-diphenyl)-1-piperazinehexanamide (LP-211) to improve in vitro microsomal stability: a case study. *Eur. J. Med. Chem.* **2016**, *120*, 363–379.
37. Huang, A.; Moretto, A.; Janz, K.; Lowe, M.; Bedard, P. W.; Tam, S.; Di, L.; Clerin, V.;

- Sushkova, N.; Tchernychev, B.; Tsao, D. H. H.; Keith Jr., J. C.; Shaw, G. D.; Schaub, R. G.; Wang, Q.; Kaila, N. Discovery of 2-[1-(4-chlorophenyl)cyclopropyl]-3-hydroxy-8-(trifluoromethyl)quinoline-4-carboxylic acid (PSI-421), a P-selectin inhibitor with improved pharmacokinetic properties and oral efficacy in models of vascular injury. *J. Med. Chem.* **2010**, *53*, 6003–6017.
38. Galley, G.; Goergler, A.; Groebke Zbinden, K.; Norcross, R. 4,5-Dihydro-oxazol-2-yl derivatives. *US2010/29589*.
39. Pivetti, F.; Fornaretto M. G.; Re M. Process for the preparation of derivatives of 1-(2-halobiphenyl-4-yl)-cyclopropanecarboxylic acid. *US2011039934*, **2011**.
40. Kirpotina, L. N.; Khlebnikov, A. I.; Schepetkin, I. A.; Ye, R. D.; Rabiet, M. J.; Jutila, M. A.; Quinn, M. T. Identification of novel small-molecule agonists for human formyl peptide receptors and pharmacophore models of their recognition. *Mol Pharmacol.* **2010**, *77*, 159–170.
41. Di, L.; Kerns, E.H.; Ma, X.J.; Huang, Y.; Carter, G.T. Applications of high throughput microsomal stability assay in drug discovery. *Comb. Chem. High Throughput Screen.* **2008**, *11*, 469–476.
42. Molteni, M.; Gemma, S.; Rossetti, C. The role of Toll-Like receptor 4 in infectious and noninfectious inflammation. *Mediators Inflamm.* **2016**, 2016:6978936.
43. Kettenmann, H.; Hanisch, U. K.; Noda, M.; Verkhratsky, A. Physiology of microglia. *Physiol. Rev.* **2011**, *91*, 461–553.
44. Rousseau, M. C.; Hsu, R. Y.; Spicer, J. D.; McDonald, B.; Chan, C. H.; Perera, R. M.; Giannias, B.; Chow, S. C.; Rousseau, S.; Law, S.; Ferri, L. E. Lipopolysaccharide-induced toll-like receptor 4 signaling enhances the migratory ability of human esophageal cancer cells in a selectin-dependent manner. *Surgery.* **2013**, *154*, 69–77.
45. Slusarczyk, J.; Trojan, E.; Glombik, K.; Piotrowska, A.; Budziszewska, B.; Kubera, M.; Popiolek-Barczyk, K.; Lason, W.; Mika, J.; Basta-Kaim A. Anti-inflammatory properties of tianeptine on lipopolysaccharide-induced changes in microglial cells involve toll-like receptor-

related pathways. *J. Neurochem.* **2016**, *136*, 958–970.

46. Džoljić, E.; Grbatinić, I.; Kostić, V. Why is nitric oxide important for our brain? *Funct. Neurol.* **2015**, *30*, 159–163.

47. Yuste, J. E.; Tarragon, E.; Campuzano, C. M., Ros-Bernal F. Implications of glial nitric oxide in neurodegenerative diseases. *Front. Cell. Neurosci.* **2015**, *9*, 322.

48. Marin, I.; Kipnis, J. Learning and memory ... and the immune system. *Learn. Mem.* **2013**, *20*, 601–606.

49. Weksler, B. B.; Subileau, E. A.; Perrière, N.; Charneau, P.; Holloway, K., Leveque, M.;

Tricoire-Leignel, H.; Nicotra, A.; Bourdoulous, S.; Turowski, P.; Male, D. K., Roux, F.;

Greenwood, J.; Romero, I. A.; Couraud, P. O. Blood-brain barrier-specific properties of a human adult brain endothelial cell line. *FASEB J.* **2005**, *19*, 1872–1874.

50. Hitchcock, S.A. Structural modifications that alter the P-glycoprotein efflux properties of compounds. *J. Med. Chem.* **2012**, *55*, 4877.

51. Ries, M.; Loiola, R.; Shah, U. N.; Gentleman, S. M.; Solito, E.; Sastre, M. The anti-inflammatory Annexin A1 induces the clearance and degradation of the amyloid- β peptide. *J. Neuroinflammation* **2016**, *13*, 234.

52. Marinier, A.; Quesnelle, C. A.; Dodier, M.; Roy, S.; Gill, P.; Wittman, M. D.; Langley, D. R. Thiazolyl compounds useful as kinase inhibitors. *US2010/048581*.

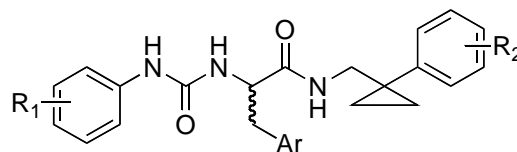
53. Obach, R. S.; Baxter, J. G.; Liston, T. E.; Silber, B. M.; Jones, B. C.; MacIntyre, F.; Rance, D. J.; Wastall, P. The prediction of human pharmacokinetic parameters from preclinical and in vitro metabolism data. *J. Pharmacol. Exp. Ther.* **1997**, *283*, 46–58.

54. Schepetkin, I. A.; Kirpotina, L. N.; Khlebnikov, A. I.; Quinn, M. T. High-throughput screening for small-molecule activators of neutrophils: Identification of novel N-formyl peptide receptor agonists. *Mol. Pharmacol.* **2007**, *71*, 1061–1074.

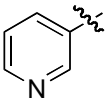
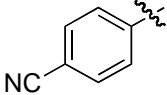
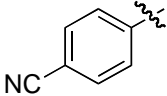
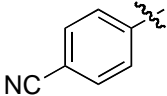
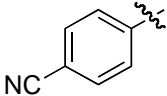
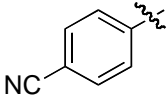
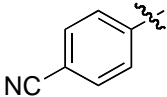
55. Riganti, C.; Salaroglio, I. C.; Pinzòn-Daza, M. L.; Caldera, V.; Campia, I.; Kopecka, J.; Mellai, M.; Annovazzi, L.; Couraud, P. O.; Bosia, A.; Ghigo, D.; Schiffer, D. Temozolomide down-

regulates P-glycoprotein in human blood-brain barrier cells by disrupting Wnt3 signaling. *Cell. Mol. Life Sci.* **2014**, *71*, 499–516.

Table 1. Effect of the compounds on Ca²⁺ mobilization in FPR1- and FPR2-HL60 transfected cells and human neutrophils, and metabolic stability.



Compd.	R ₁	Ar	R ₂	EC ₅₀ , μM (Efficacy %)			Metabolic stability (% remaining) ^a
				FPR2-HL60	FPR1-HL60	Neutrophils	
5				0.26 ^b	0.19 ^b	0.086 ^b	4
(<i>R</i>)-6	NO ₂		H	N.A. ^b	N.A. ^b	N.A. ^b	15
(<i>S</i>)-6				7.6 ± 2.1 (60) ^b	N.A. ^b	N.A. ^b	11
(<i>R</i>)-7	OCH ₃		H	6.5 ± 1.8 (55)	N.A.	N.A.	4
(<i>S</i>)-7				0.11 ± 0.03 (125)	0.95 ± 0.3 (105)	1.4 ± 0.3 (145)	3
(<i>R</i>)-8	F		H	N.A.	N.A.	N.A.	4
(<i>S</i>)-8				2.0 ± 0.4 (70)	18.8 ± 3.7 (60)	N.A.	4
(<i>R</i>)-9	H		H	N.A.	N.A.	N.A.	4
(<i>S</i>)-9				6.7 ± 1.9 (35)	2.4 ± 0.7 (55)	1.5 ± 0.4 (25)	5
(<i>R</i>)-10	NO ₂		H	1.5 ± 0.3 (90)	4.7 ± 1.1 (75)	4.1 ± 0.8 (150)	38
(<i>S</i>)-10				0.63 ± 0.2 (100)	2.8 ± 0.6 (75)	2.5 ± 0.7 (115)	56

(<i>R</i>)-11	NO ₂		H	2.9 ± 0.8 (60)	1.5 ± 0.4 (145)	0.12 ± 0.04 (90)	45
(<i>S</i>)-11				6.4 ± 1.5 (60)	0.85 ± 0.3 (125)	0.73 ± 0.2 (65)	51
(<i>R</i>)-12	OCH ₃		OCF ₃	N.A.	N.A.	N.A.	43
(<i>S</i>)-12				N.A.	N.A.	N.A.	51
(<i>R</i>)-13	F		OCF ₃	N.A.	N.A.	N.A.	88
(<i>S</i>)-13				N.A.	N.A.	N.A.	80
(<i>R</i>)-14	OCH ₃		4-CH ₃ - 3-F	N.A.	N.A.	N.A.	10
(<i>S</i>)-14				16.3 ± 3.6 (35)	10.3 ± 2.2 (55)	1.7 ± 0.4 (70)	8
(<i>R</i>)-15	F		4-CH ₃ - 3-F	N.A.	N.A.	N.A.	37
(<i>S</i>)-15				3.0 ± 0.8 (65)	5.9 ± 1.6 (50)	1.7 ± 0.5 (55)	39
(<i>R</i>)-16	OCH ₃		3-Cl-4- F	1.8 ± 0.3 (60)	0.63 ± 0.2 (100)	0.73 ± 0.2 (115)	5
(<i>S</i>)-16				3.4 ± 0.9 (60)	0.45 ± 0.1 (115)	0.33 ± 0.1 (155)	10
(<i>R</i>)-17	F		3-Cl-4- F	0.3 ± 0.1 (90)	5.4 ± 1.2 (55)	1.3 ± 0.4 (95)	20
(<i>S</i>)-17				3.9 ± 1.1 (80)	5.2 ± 1.4 (55)	0.19 ± 0.05 (130)	33

^aPercent of parent compound remaining after 30-min incubation. ^bData taken from ref. 32.

Table 2. Half-life and Intrinsic Clearance of Selected Compounds.

Compound	t_{1/2} (min)	CL_{int} (μL/min/mg)
5	1.1 ^a	1162.4 ^a
<i>(R)</i> - 10	95	7.29
<i>(S)</i> - 10	120	5.78
<i>(R)</i> - 11	99	7.0
<i>(S)</i> - 11	110	6.3
<i>(R)</i> - 17	47	14.7
<i>(S)</i> - 17	48	14.4
<i>(R)</i> - 15	59	10.04

^aData taken from ref. 33.

Table 3. Bidirectional Transport across hCMEC/D3 Cells of Compounds (*S*)-**10**, (*R*)-**11**, and (*S*)-**17**.

Compound	P_{app}BA (nm/sec)^a	P_{app}AB (nm/sec)^b	ER(BA/AB)
(<i>S</i>)- 10	253033	49785	5.06
(<i>R</i>)- 11	437544	119245	3.7
(<i>S</i>)- 17	375981	145521	2.6

^aApparent permeability of the basolateral-to-apical transport; ^bApparent permeability of the apical-to-basolateral transport.

Chart 1. Structural Formulas of Non-Peptidic FPR2 Agonists

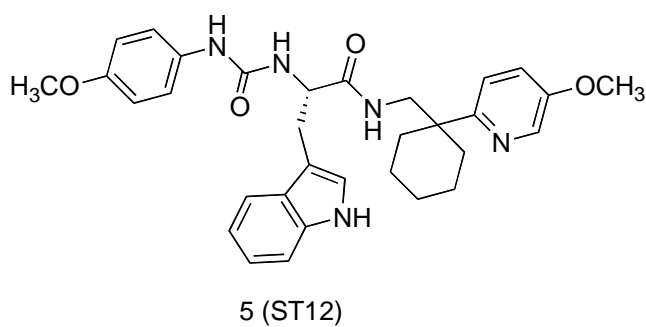
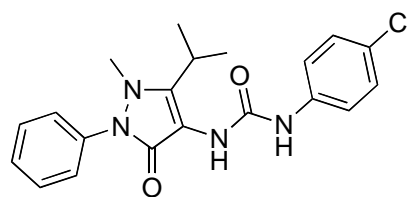
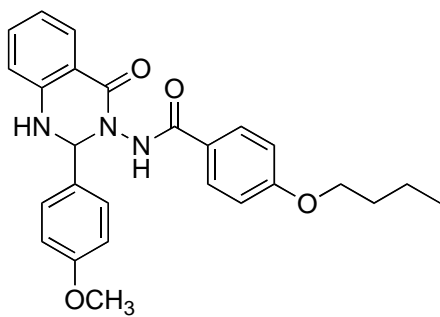
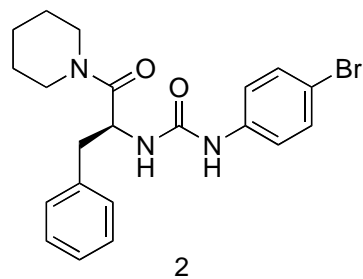
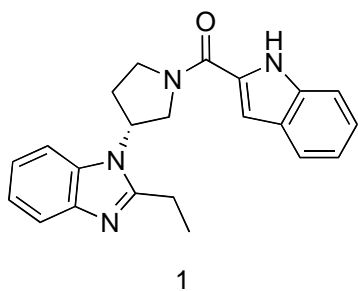
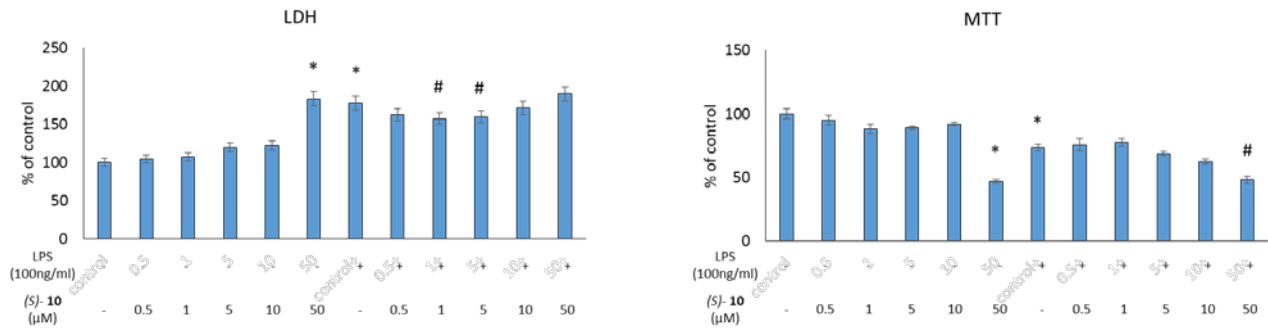
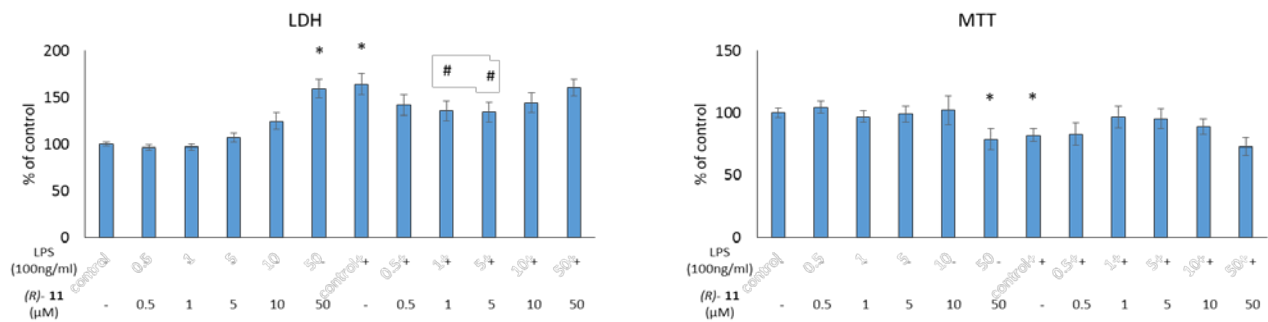


Figure 1. Effect of the (*S*)-**10** (A), (*R*)-**11** (B) and (*S*)-**17** (C) in LDH and MTT assays in rat microglial cell cultures.

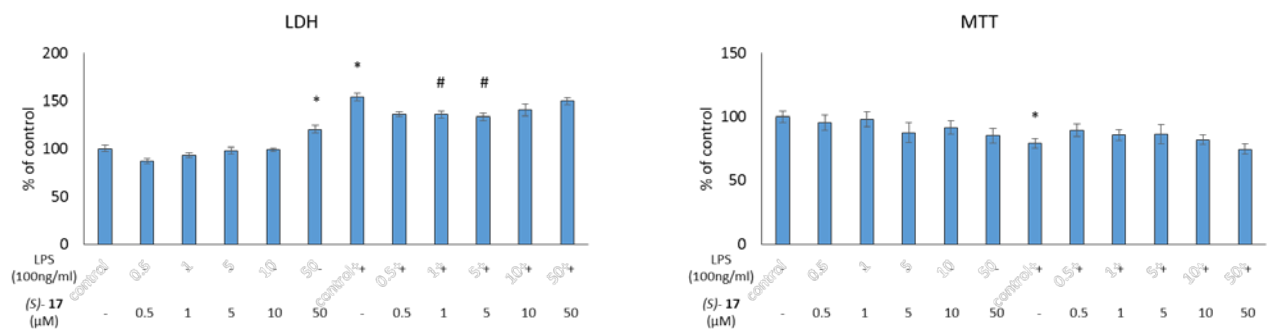
A)



B)

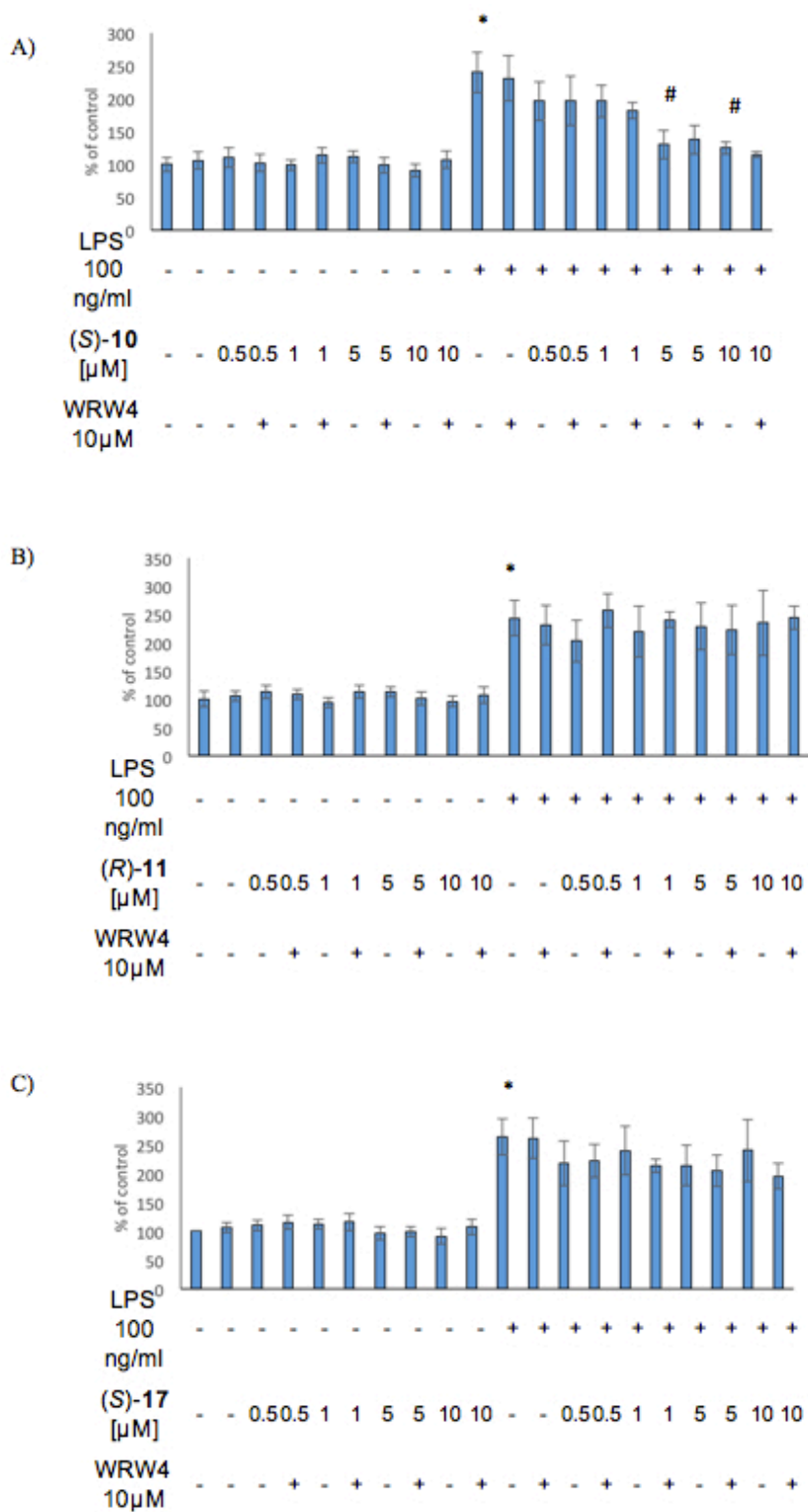


C)



* vs control
vs control + LPS

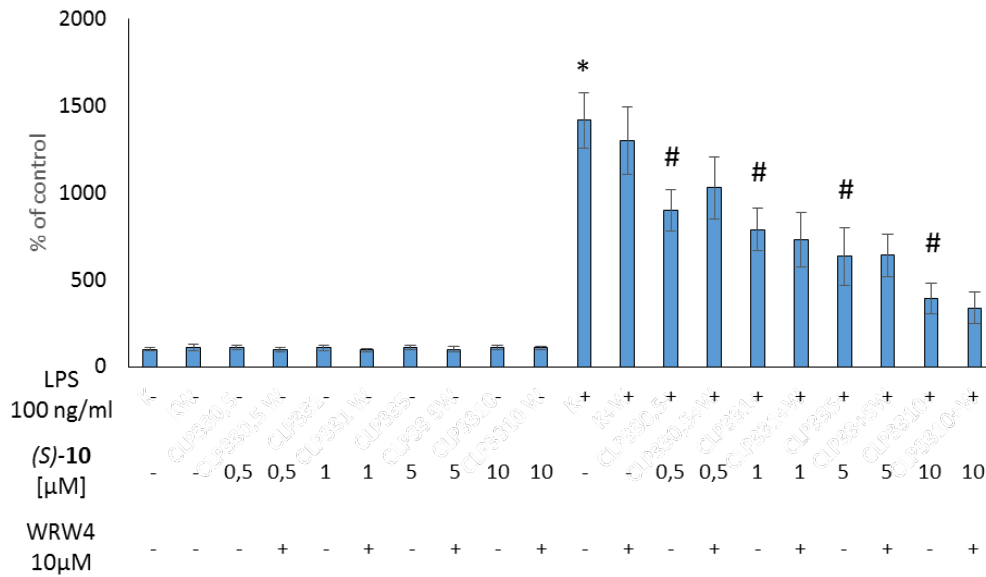
Figure 2. Effect of the (*S*)-**10** (A), (*R*)-**11** (B) and (*S*)-**17** (C) on NO production assays in rat microglial cell cultures.



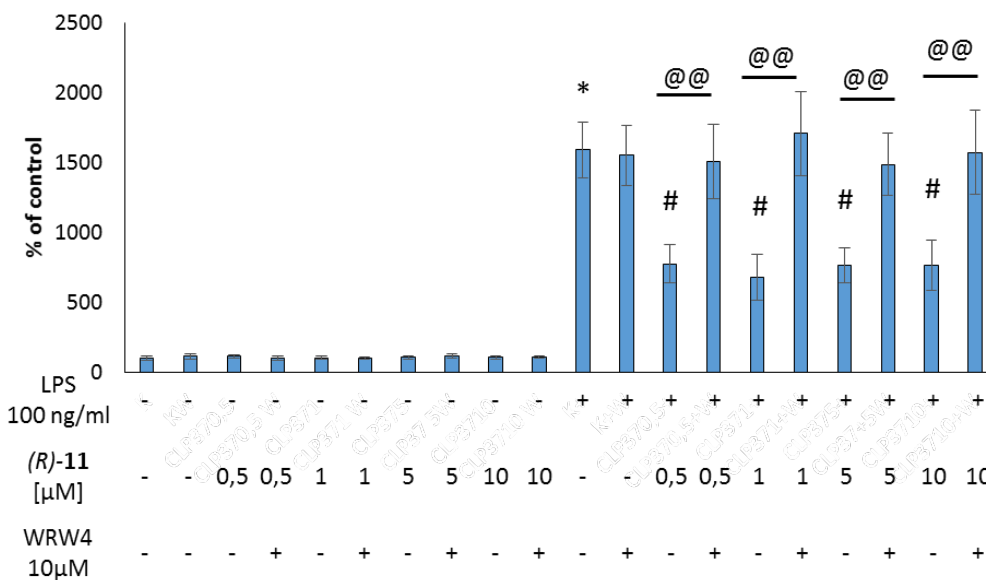
* vs control
vs control + LPS

Figure 3. Effect of the (*S*)-**10** (A), (*R*)-**11** (B) and (*S*)-**17** (C) on IL-1 β production assays in rat microglial cell cultures. – Dovrebbe essere scritto 0.5 al posto di 0,5 in questa figura

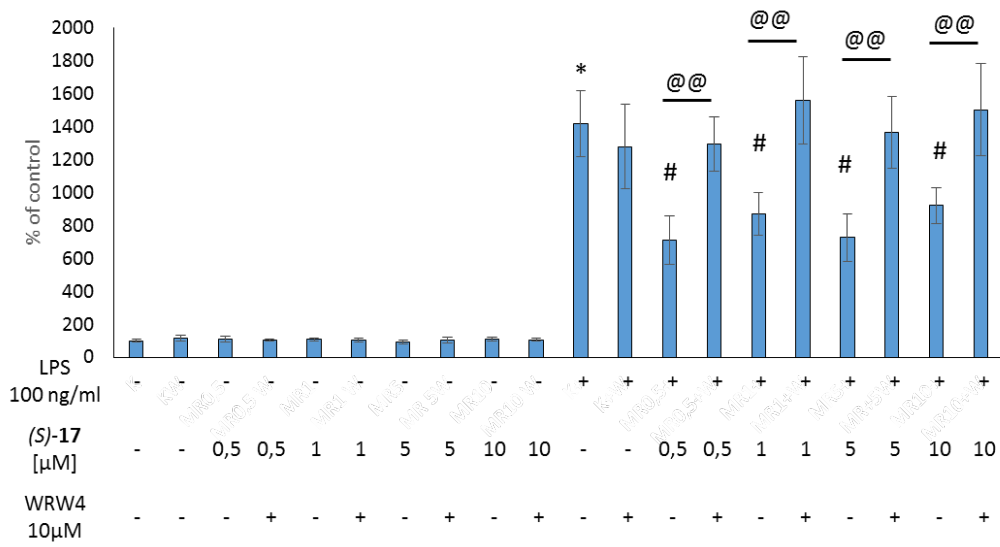
A)



B)



C)



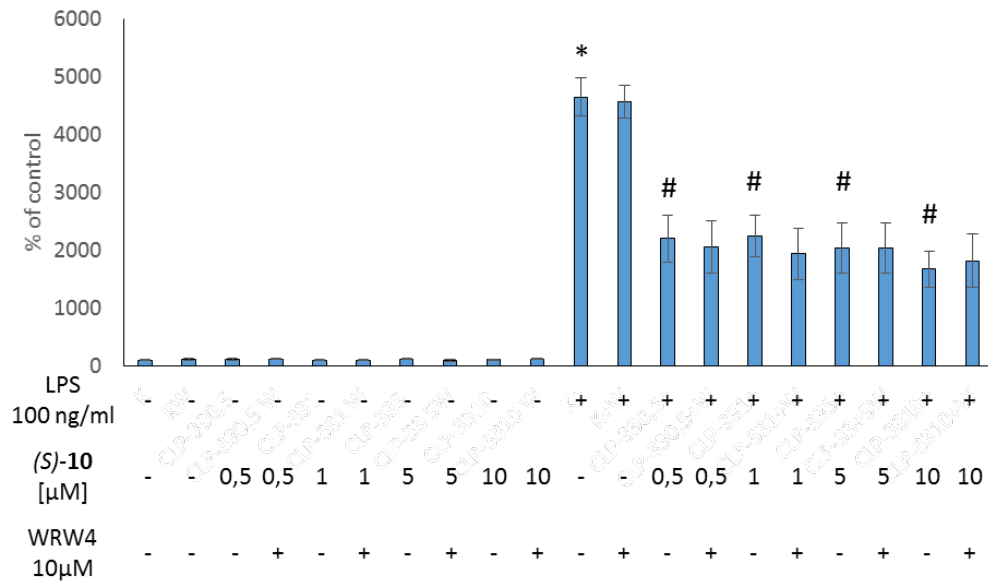
* vs control

vs control + LPS

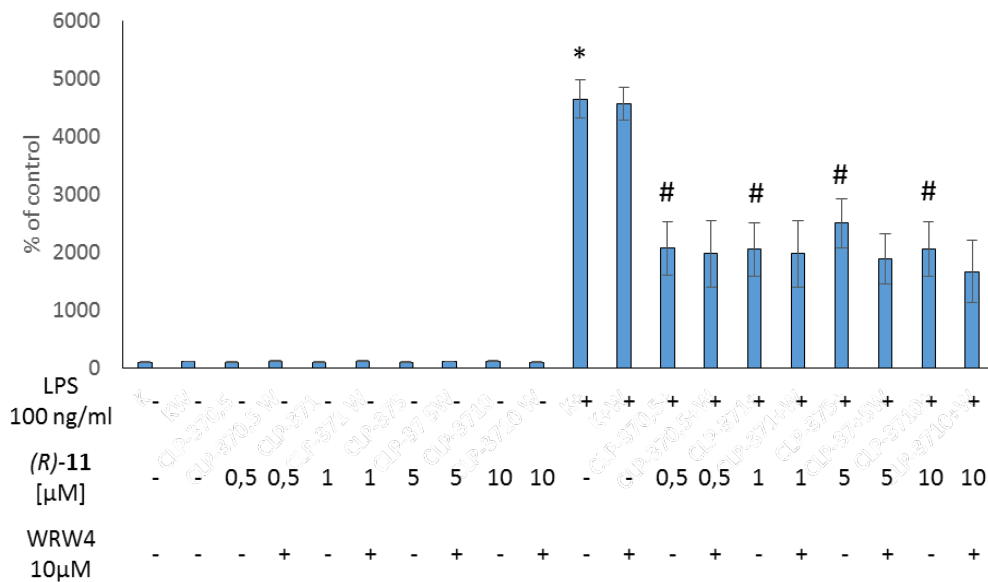
@@ vs agonist + LPS

Figure 4. Effect of the (*S*)-10 (A), (*R*)-11 (B) and (*S*)-17 (C) on TNF- α production assays in rat microglial cell cultures. Dovrebbe essere scritto 0.5 al posto di 0,5 in questa figura

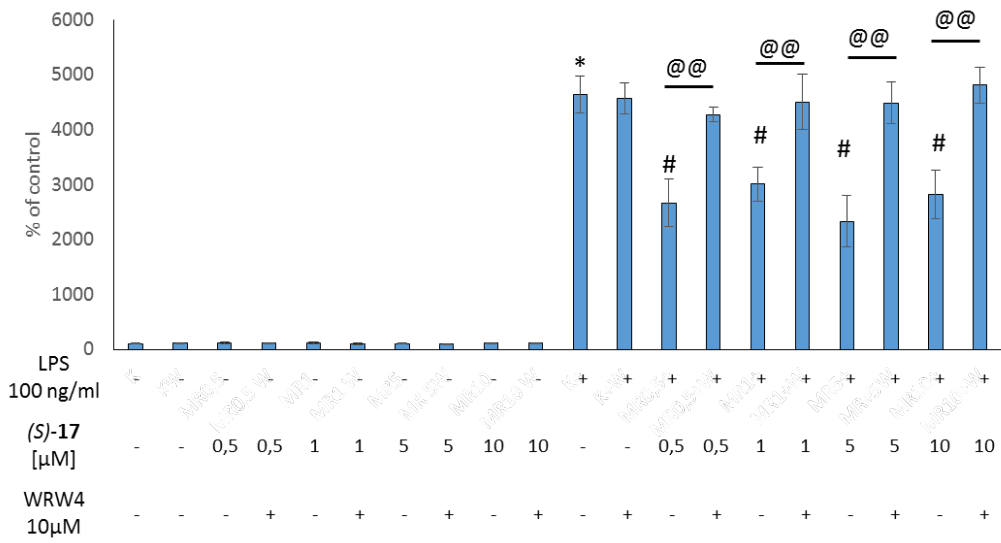
A)



B)



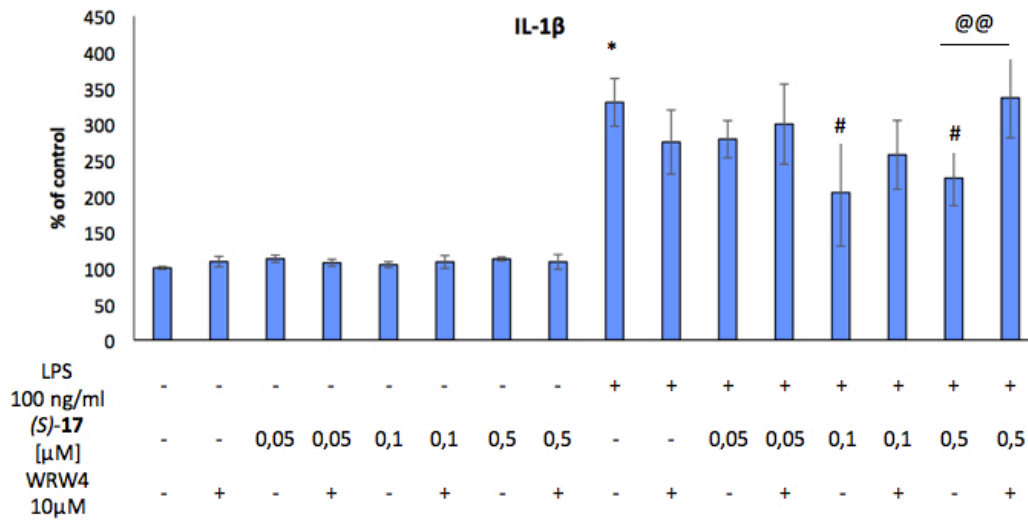
C)



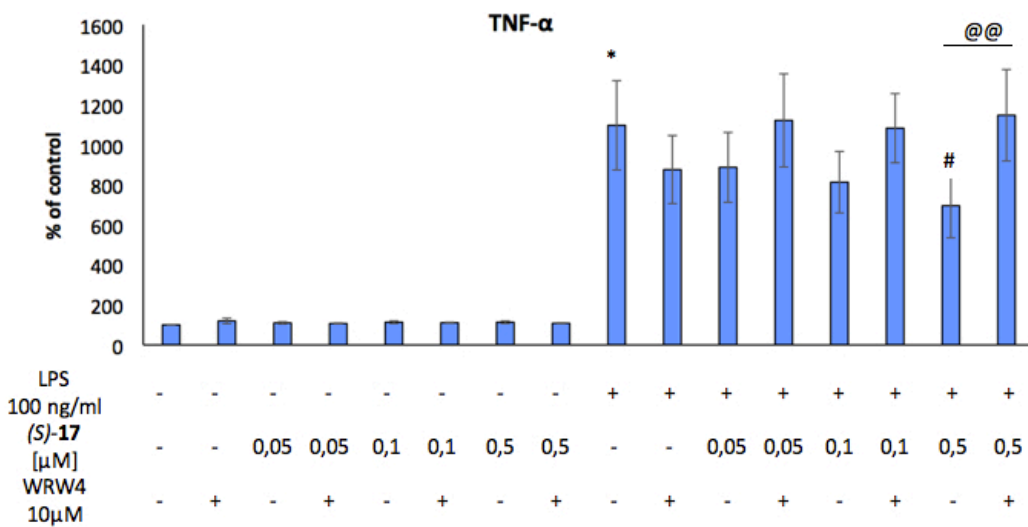
* vs control
 # vs control + LPS
 @@ vs agonist + LPS

Figure 5. Effect of low doses of (*S*)-**17** on IL-1 β (A) and TNF- α (B) production assays in rat microglial cell cultures. Dovrebbe essere scritto 0.5 al posto di 0,5 in questa figura

A)



B)

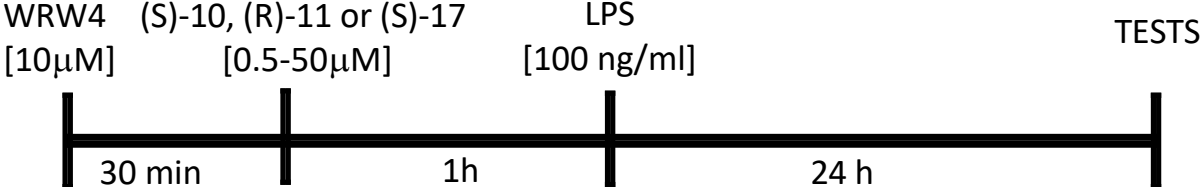


* vs control

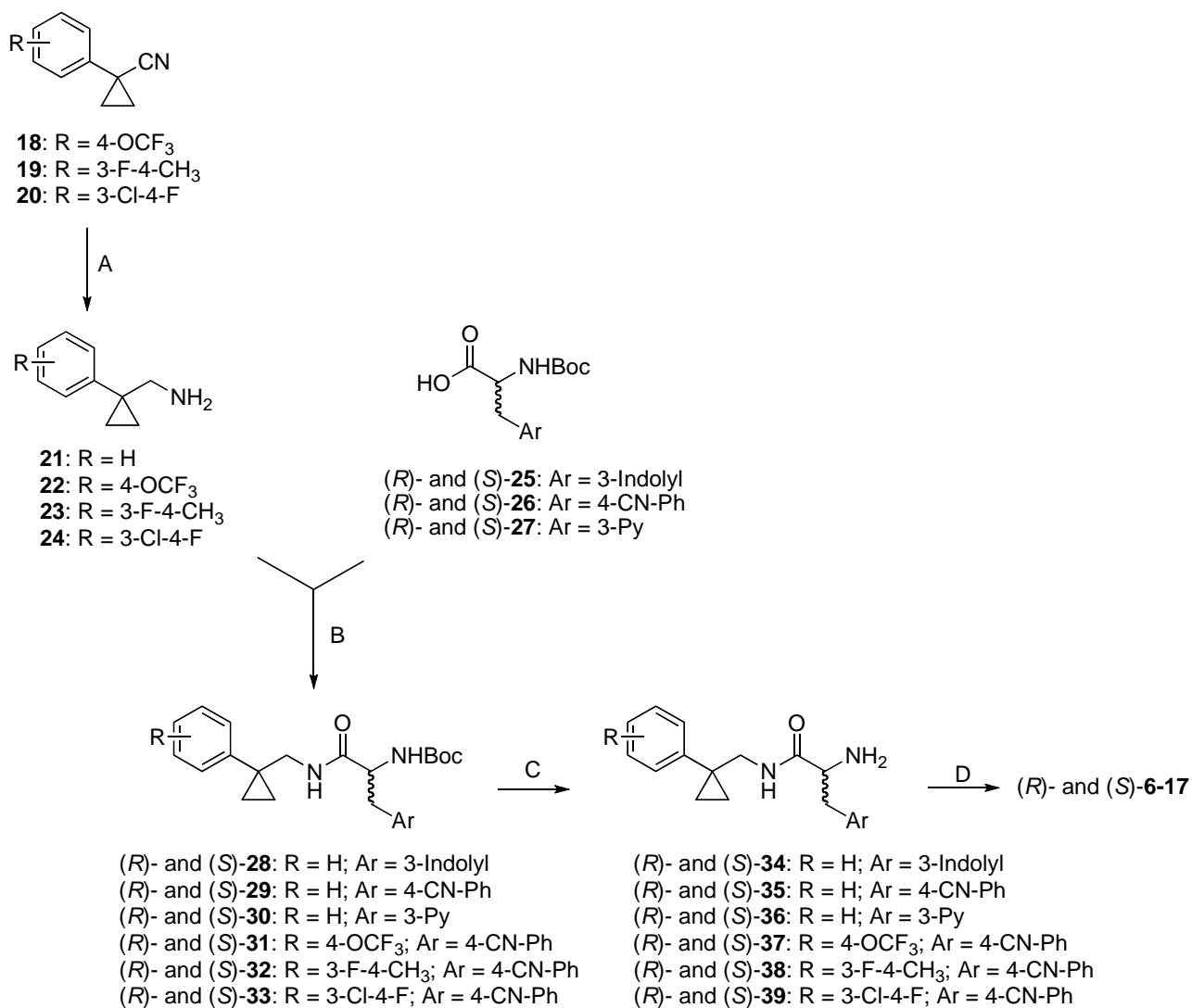
vs control + LPS

@@ vs agonist + LPS

Figure 6. Schematic Diagram Representing the Schedule of the Experiments on Rat Primary Microglial Cell Cultures.



Scheme 1. Synthesis of the target compounds (*R*)- and (*S*)-**6-17**.



“Reagents and Conditions: (A) Raney-nickel, H₂, 2 M ethanolic NH₃; 5 atm; 50 °C, 15 h, 77-90% yield or borane-methyl sulfide complex 10 M, HCl, 81% yield; (B) *N,N'*-carbonyldiimidazole, r.t., overnight, 45-87% yield; (C) trifluoroacetic acid, r.t., 5 h, quantitative yield; (D) 4-substituted phenylisocyanate, r.t., overnight, 10-80% yield; or 4-substituted aniline, *N,N'*-carbonyldiimidazole, r.t., overnight, 10-19% yield.

Table of Contents Graphic

